

The Role of Plasma Heating and Expansion in the Energetics of Solar Coronal Mass Ejections

A Thesis

submitted to

Indian Institute of Science Education and Research Pune
in partial fulfillment of the requirements for the
BS-MS Dual Degree Programme

by

Niranjana Thejaswi S



Indian Institute of Science Education and Research Pune
Dr. Homi Bhabha Road,
Pashan, Pune 411008, INDIA.

April, 2019

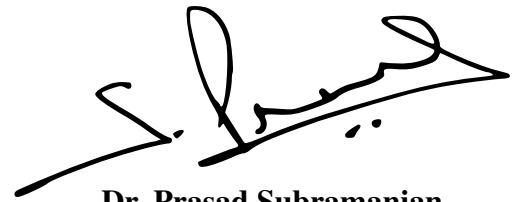
Supervisor: **Dr. Prasad Subramanian**

© **Niranjana Thejaswi S** 2019

All rights reserved

Certificate

This is to certify that this dissertation entitled **The Role of Plasma Heating and Expansion in the Energetics of Solar Coronal Mass Ejections** towards the partial fulfilment of the BS-MS dual degree programme at the Indian Institute of Science Education and Research, Pune represents study/work carried out by **Niranjana Thejaswi S** at Indian Institute of Science Education and Research under the supervision of **Dr. Prasad Subramanian**, Associate Professor, Department of Physics , during the academic year 2018-2019.

A handwritten signature in black ink, appearing to read 'Prasad Subramanian', with a long horizontal stroke extending to the right.

Dr. Prasad Subramanian

Committee:

Dr. Prasad Subramanian

Dr. Arijit Bhattacharyay

This thesis is dedicated to my grandparents

Declaration

I hereby declare that the matter embodied in the report entitled **The Role of Plasma Heating and Expansion in the Energetics of Solar Coronal Mass Ejections** are the results of the work carried out by me at the Department of Physics, Indian Institute of Science Education and Research, Pune, under the supervision of **Dr. Prasad Subramanian** and the same has not been submitted elsewhere for any other degree.

S.N.Thejaswi

Niranjana Thejaswi S

Acknowledgments

I express my deep gratitude to my supervisor, Prof. Prasad Subramanian for patiently guiding and encouraging me throughout my thesis. His profound understanding of the subject has aided me in finding a direction to my thesis and to circumvent problems. I thank Prof. Arijit Bhattacharyay for supporting me as my TAC member.

I am thankful to Debesh Bhattacharjee for numerous discussions and support throughout my thesis. I am grateful to Dr. Nishtha Sachdeva whose previous work with Prof. Prasad was foundational to my thesis and also for her valuable suggestions.

I thank my parents who have continuously supported me throughout my life and have encouraged me to pursue all the things that I wished to. Last, but not the least, I thank all my friends who have made my life cheerful and colourful.

Abstract

Coronal Mass Ejections (CMEs) are bodily expulsions of hot plasma and magnetic fields from the solar corona. Such ejections, which are often directed towards the Earth cause geomagnetic storms, which substantially affect technologies we use on a routine basis. This has prompted extensive investigations of the manner in which CMEs are initiated in the solar corona and the manner in which they propagate through the heliosphere. However, there has not been as much attention devoted to the energy expended in expanding and heating the CME as it propagates. These are crucial issues, the answers to which can substantially impact our understanding of CME dynamics.

Were the CMEs to expand adiabatically from near the sun to the earth, then their temperature would be no more than a few degrees of kelvin. But the observed temperatures of CME plasma intercepted near the Earth are around a hundred thousand kelvin. Furthermore, our understanding of laboratory tokamak plasmas suggests that expanding magnetic flux ropes (such as CMEs) should contract in cross-section, whereas CMEs are observed to expand. These suggest that our understanding of CME driving and thermodynamics is far from complete.

We examine a well-observed set of CMEs that have been tracked from their origin at the Sun to their interception at the Earth. We seek to reconcile their propagation and expansion profiles in the context of a flux rope model that accounts for Lorentz forces as well as gas pressure. We obtain observationally motivated constraints on the evolution of temperature, polytropic index and plasma beta of these CMEs. These results can also allow us to investigate how turbulent fluctuations inside the CME are possibly dissipated. Taken together, our results are expected to provide inputs to an operational model of CME propagation from the Sun to the Earth.

Contents

Abstract	xi
1 Introduction	1
1.1 Coronal Mass Ejections	1
1.2 Energetics of CME	2
1.3 Importance	3
1.4 CME Morphology	4
2 Lorentz Force	7
2.1 Lorentz Force in MHD	7
2.2 Resolving Lorentz Force	8
2.3 Magnetic Tension and Pressure Forces	10
3 CME Dynamics	11
3.1 Effect of Lorentz force	11
3.2 Major Radial Force Equation	13
3.3 Minor Radial Force Equation	18
4 Force-free Approximation	21

4.1	Motivation	21
4.2	Force-free Configuration	22
4.3	Lundquist Solution	23
5	Analysis	25
5.1	Data From GCS Fitting	25
5.2	Estimation of Expressions of β_p , Pressure and Temperature	28
5.3	Estimation of Magnetic Field Profile	33
5.4	Inconsistencies due to differences in two models: Torus Instability Model (Kleim and Torok) and Flux Injection Model (Chen)	34
5.5	Estimation of Polytropic Index and Heating Rates	39
5.6	Estimation of CME Temperature at 1 AU for an Adiabatic Expansion	41
6	Results and Discussions	43
6.1	Temperature Profiles	43
6.2	Polytropic Index	45
6.3	β_p and Plasma Beta Profiles	46
6.4	Magnetic Field Profiles	49
6.5	Pressure Profiles	51
6.6	Heating Budget and Rates	52
7	Conclusions	55
8	Appendix	57
8.1	Another Method to Estimate β_p and Temperature Profiles	57
8.2	Correction to Force-free Solutions	60

8.3 Mathematica Codes 61

List of Figures

1.1	CME on February, 2000	2
1.2	Model of a CME torus	4
3.1	Contraction of cross-section	12
3.2	Expansion of length	12
3.3	Effect of Lorentz force on a CME torus	12
3.4	$J_p \times B_t$ force realised by Magnetic tension force	15
3.5	Relation between radial and tangential forces in cylindrical symmetry	16
4.1	Force-free helical magnetic fields, solutions to cylindrical symmetry	24
4.2	Force-free helical magnetic fields embedded in a CME torus	24
5.1	Extrapolation by fitting $a(b^{cx}) + d$	34
5.2	Extrapolation by fitting $a(x^b)$	34
6.1	CME 1 - Temperature profile	44
6.2	CME 5 - Temperature profile	44
6.3	CME 9 - Temperature profile	44
6.4	CME 20 - Temperature profile	44
6.5	CME 33 - Temperature profile	44

6.6	CME 36 - Temperature profile	44
6.7	CME 1 - Polytropic Index fit	45
6.8	CME 5 - Polytropic Index fit	45
6.9	CME 9 - Polytropic Index fit	45
6.10	CME 20 - Polytropic Index fit	45
6.11	CME 33 - Polytropic Index fit	45
6.12	CME 36 - Polytropic Index fit	45
6.13	Histogram of polytropic index	46
6.14	CME 1 - β_p profile	47
6.15	CME 5 - β_p profile	47
6.16	CME 9 - β_p profile	47
6.17	CME20 - β_p profile	47
6.18	CME 33 - β_p profiles	47
6.19	CME 36 - β_p profile	47
6.20	CME 1 - Plasma beta profile	48
6.21	CME 5 - Plasma beta profile	48
6.22	CME 9 - Plasma beta profile	48
6.23	CME 20 - Plasma beta profile	48
6.24	CME 33 - Plasma beta profile	48
6.25	CME 36 - Plasma beta profile	48
6.26	CME 1 - Magnetic field profile	49
6.27	CME 2 - Magnetic field profile	49
6.28	CME 3 - Magnetic field profile	49
6.29	CME 4 - Magnetic field profile	49

6.30	CME 5 - Magnetic field profile	49
6.31	CME 11 - Magnetic field profile	49
6.32	Histogram: Error in extrapolated B values	50
6.33	CME 1 - Pressure profile	51
6.34	CME 5 - Pressure profile	51
6.35	CME 9 - Pressure profile	51
6.36	CME 20 - Pressure profile	51
6.37	CME 33 - Pressure profile	51
6.38	CME 36 - Pressure profile	51
6.39	CME 1 - Heating Rate	52
6.40	CME 5 - Heating Rate	52
6.41	CME 9 - Heating Rate	52
6.42	CME 20 - Heating Rate	52
6.43	CME 33 - Heating Rate	52
6.44	CME 36 - Heating Rate	52
8.1	7th order polynomial fit to find acceleration	59
8.2	11th order polynomial fit to find acceleration	59
8.3	15th order polynomial fit to find acceleration	59
8.4	Curvature of helical fields due to curvature of CME torus	60
8.5	Non-overlapping adjacent rings of magnetic field due to curvature of CME torus	60

List of Tables

5.1 CME parameters	27
------------------------------	----

Chapter 1

Introduction

1.1 Coronal Mass Ejections

Corona is a region of hot plasma outside the photosphere of the sun. Temperature of the corona is unusually high, even higher than the photosphere. Corona contains highly twisted strong magnetic fields, storing huge amounts of energy. The high temperature is possibly due to the dissipation of this magnetic energy. At times, oppositely directed field lines could come close to each other, and there could be a realignment of field lines accompanied with release of high amounts of energy and expulsion of plasma from corona. This process is called magnetic reconnection [21], which would relieve stress in the highly twisted magnetic fields.

Coronal Mass Ejections (CMEs) are such bodily expulsions of hot plasma and magnetic fields from the solar corona into the interplanetary space. They have a typical mass of around 10^{15} grams and contain energy of about 10^{30} ergs. They move through the heliosphere at velocities of several hundred kilometres per second (Howard [11]). They occur a few times every day. They can be studied using white light coronagraphs and in-situ observations through satellites.

CMEs which are at a larger distance from the sun propagating through heliosphere are termed as Interplanetary CMEs (ICMEs). When these ICMEs pass through a spacecraft, an increase in the intensity of the magnetic field, where the field varies smoothly with time is observed. These manifestations of ICMEs are called magnetic clouds (Burlaga [5])

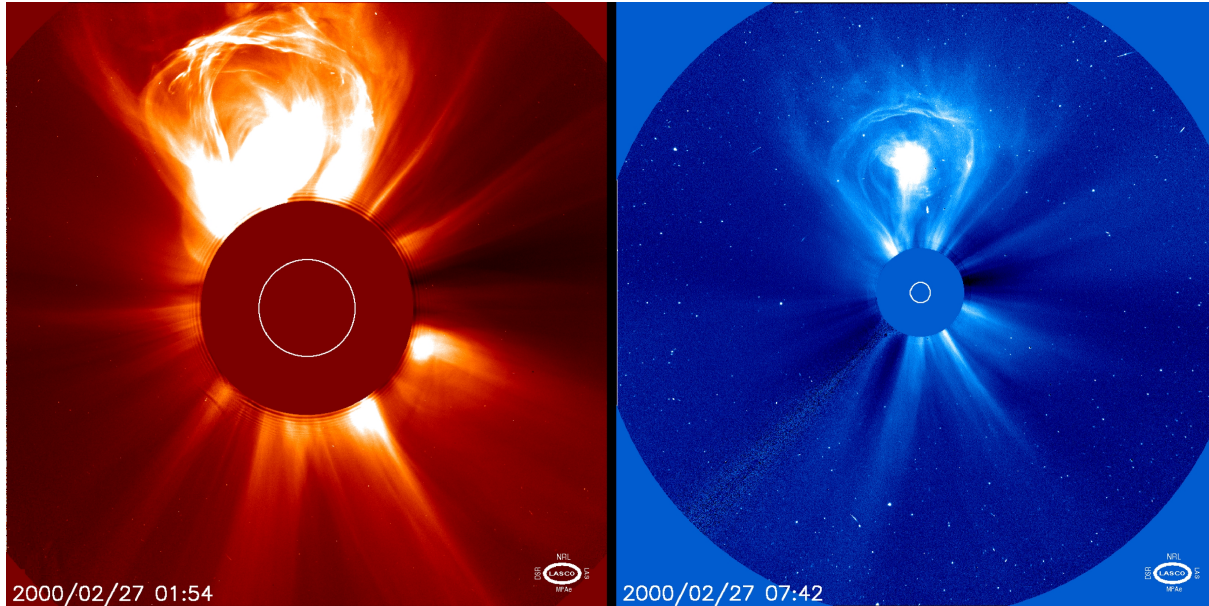


Figure 1.1: An image of a CME on February, 2000 from the LASCO coronagraph on board SOHO. In coronagraph, a disc occults the sun. **Credits:** <https://sohowww.nascom.nasa.gov/>

1.2 Energetics of CME

CMEs are observed to augment in length and cross-section as they propagate away from the sun. The increase in length is termed as translation and the increase in the cross-section is termed as expansion. As the CME erupts and propagates through the heliosphere energy is required to do work against the gravitational potential energy and to provide kinetic energy and energy for expansion. This energy is possibly accounted by the high energy stored in the magnetic fields. The energy stored in magnetic field before erupting is an order of magnitude higher than the required amount of other energies mentioned above (Forbes [9]). Kumar and Rust [13] have shown that assumption of magnetic helicity and flux in self-similarly evolving flux ropes leads to a monotonous decrease in magnetic energy as the CME propagates.

Chen and Garren (1993) [10] estimate that if the CME were to expand adiabatically, then the near earth temperature would be a few degrees of kelvin. I have also done a similar estimate in a later section 5.6. But the observed temperatures are about a million-degree kelvin. This indicates that there is local heating of plasma. The source for this plasma heating is again magnetic energy. They suggest that about 58-78 per cent of magnetic energy could be used up in heating CME plasma. Liu et al. [16] state that turbulent dissipation of magnetic fields is sufficient to account for CME

plasma heating. They also suggest a polytropic index of about 1.3 at distances between 0.3 and 20 AU

We have obtained temperature, pressure, plasma beta and density profiles of a set of well-observed CMEs. We can further estimate heating budgets and rates as a function of heliospheric distance. We also have an estimate of polytropic index of these CMEs.

1.3 Importance

CMEs, which are often directed towards the Earth interact with earth's magnetic field to cause geomagnetic storms. These storms substantially affect the technologies we use on a routine basis.

- They can induce currents in long transmission wires and damage them [4]. CMEs with very high magnetic fields can damage power grids which could cause electrical blackouts for weeks or even months.
- Radio communications depend on the ionosphere to reflect radio waves. CMEs can drive storms in the ionosphere of earth's atmosphere leading to fluctuating signals and disrupting radio communication.
- Geomagnetic storms can heat earth's upper atmosphere, leading to an increase in density of air near satellites, which in turn causes increased drag force on satellites. Due to this, satellites may go off orbit and may slowly fall and burn. The shocks due to CMEs can produce energetic particles at near-relativistic energies. These particles can physically damage sensitive components of satellites and can charge satellite components, destroying them.
- They affect navigation systems like GPS by disrupting its signal propagation through the ionosphere.
- They also pose a threat of elevated radiation exposure to astronauts and aircraft.

We can conclude that CMEs have the potential to cause billions of dollars of damage to our technologies and considerably disrupt human life. Hence, it is very important to focus our attention on their research. A good understanding of their energetics is necessary for reliable space weather conditions.

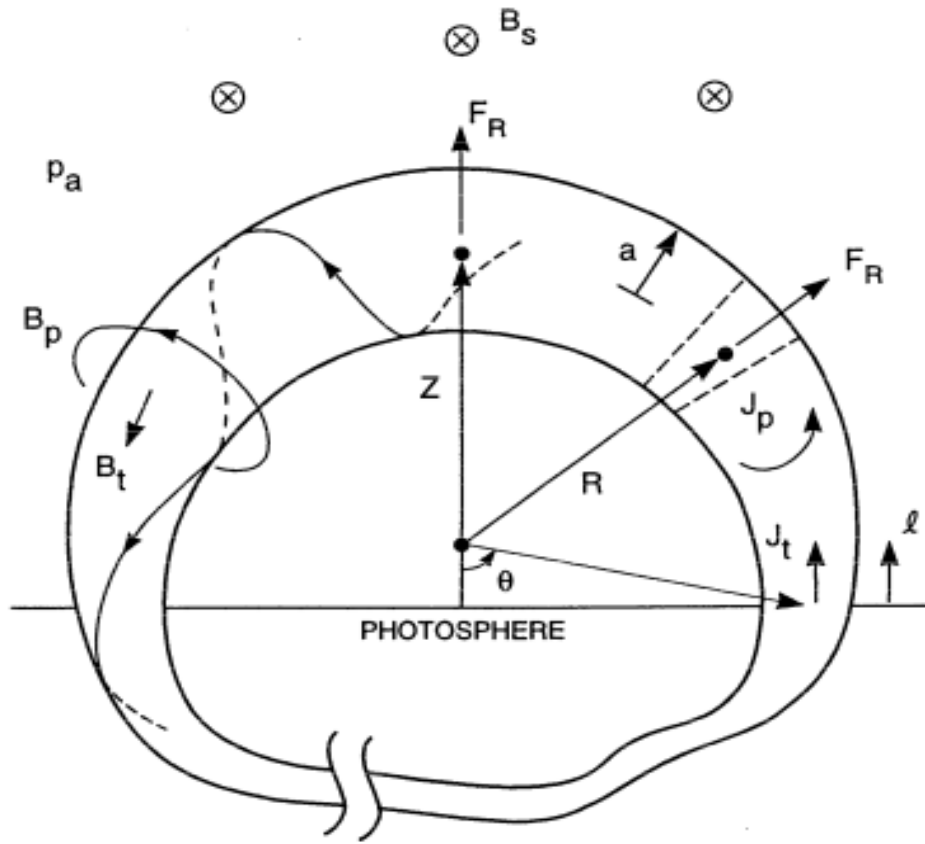


Figure 1.2: CME as a toroidal flux rope with tapering ends submerged in the photosphere **Credits:** Chen 1989[7], 1996[6]

1.4 CME Morphology

We model a fully formed CME propagating through the heliosphere as a torus with tapering ends, with the foots submerged in the photosphere. Helical magnetic fields are embedded in this torus. We use the model used by Chen, 1996 [6].

- B_t and B_p are the toroidal and poloidal magnetic fields
- J_t and J_p are the toroidal and poloidal current densities
- a and R are the minor and major radii of the CME
- B_s is the external poloidal magnetic field, p_a is the ambient solar wind pressure

Chapter 2

Lorentz Force

Lorentz force is the major force which governs the dynamics of CMEs. In electrodynamics Lorentz force on charge dq is given by (in cgs units),

$$df = dq(E + \frac{v}{c} \times B)$$

Lorentz force density on charge distribution with density ρ is given by,

$$F = \rho(E + \frac{v}{c} \times B)$$

Current density is expressed as $j = \rho v$. Hence Lorentz force density can be expressed as

$$F = \rho E + \frac{j \times B}{c}$$

2.1 Lorentz Force in MHD

In MHD approximation, the plasma is assumed to have infinite conductivity. This is a good approximation for astrophysical plasmas as they have a very high conductivity. In such plasmas, the electric field is zero in the rest frame of the plasma. The equations for Lorentz transformations of electric field components (parallel and perpendicular to plasma velocity) from rest frame of plasma

(S') to the frame of observer (S), with respect to whom, plasma is moving with a velocity, v

$$E'_{\parallel} = E_{\parallel}$$

$$E'_{\perp} = \gamma \left(E_{\perp} + \frac{v \times B}{c} \right)$$

Substituting $E'_{\parallel} = E'_{\perp} = 0$, gives us

$$E = -\frac{v \times B}{c}$$

With the expression for Electric field, the following Maxwell's equation is modified as,

$$4\pi j + \frac{\partial E}{\partial t} = c(\nabla \times B) \implies 4\pi j + \frac{\partial}{\partial t} \left(\frac{v \times B}{c} \right) = c(\nabla \times B)$$

In the non relativistic limit ($v/c \ll 1$), We can neglect the second term of the LHS in the modified equation

$$4\pi j = c(\nabla \times B) \implies j = \frac{c}{4\pi}(\nabla \times B)$$

Also, we consider plasma to be neutral overall i.e net charge density of a considerable volume of plasma, ρ is 0. Lorentz force density is given by,

$$F = \frac{j \times B}{c} \implies \frac{1}{4\pi}(\nabla \times B) \times B \quad (2.1)$$

We can observe that Lorentz force has changed from being a force on moving charges due to magnetic field to a force with a tensorial nature under MHD approximation

2.2 Resolving Lorentz Force

We use the following vector identity to resolve Lorentz force,

$$\nabla(\mathbf{a} \cdot \mathbf{b}) = (\mathbf{a} \cdot \nabla)\mathbf{b} + (\mathbf{b} \cdot \nabla)\mathbf{a} + \mathbf{a} \times (\nabla \times \mathbf{b}) + \mathbf{b} \times (\nabla \times \mathbf{a})$$

Here both vectors \mathbf{a} and \mathbf{b} are replaced with magnetic field vector \mathbf{B} .

$$\nabla(\vec{B} \cdot \vec{B}) = (\vec{B} \cdot \nabla)\vec{B} + (\vec{B} \cdot \nabla)\vec{B} + \vec{B} \times (\nabla \times \vec{B}) + \vec{B} \times (\nabla \times \vec{B})$$

$$\begin{aligned}\implies \nabla(\vec{B} \cdot \vec{B}) &= (\vec{B} \cdot \nabla)\vec{B} + (\vec{B} \cdot \nabla)\vec{B} - (\nabla \times \vec{B}) \times \vec{B} - (\nabla \times \vec{B}) \times \vec{B} \\ \implies 2(\nabla \times \vec{B}) \times \vec{B} &= 2(\vec{B} \cdot \nabla)\vec{B} - \nabla(B^2)\end{aligned}$$

Therefore, substituting the above expression in 2.1, we have,

$$F = \frac{1}{4\pi}(\nabla \times \vec{B}) \times \vec{B} = \frac{1}{4\pi}(\vec{B} \cdot \nabla)\vec{B} - \frac{1}{8\pi}\nabla B^2 \quad (2.2)$$

Now decompose magnetic field vector $\vec{B} = B\hat{s}$, where \hat{s} is the unit vector along the direction of B and $B = |\vec{B}|$. The First term in the above equation becomes

$$(\vec{B} \cdot \nabla)\vec{B} = (B\hat{s} \cdot \nabla)B\hat{s} = B(\hat{s} \cdot \nabla B)\hat{s} + B^2(\hat{s} \cdot \nabla)\hat{s} \quad (2.3)$$

The first term on the RHS of the expression can again be resolved as follows

$$B(\hat{s} \cdot \nabla B)\hat{s} = (\hat{s} \cdot (B\nabla B))\hat{s} = (\hat{s} \cdot \frac{1}{2}\nabla B^2)\hat{s}$$

Equation 2.3 now becomes,

$$(B\hat{s} \cdot \nabla)B\hat{s} = (\hat{s} \cdot \frac{1}{2}\nabla B^2)\hat{s} + B^2(\hat{s} \cdot \nabla)\hat{s}$$

Substituting the above expression in 2.2

$$\begin{aligned}F &= \frac{1}{4\pi}(\frac{1}{2}\hat{s}(\hat{s} \cdot \nabla B^2) + B^2(\hat{s} \cdot \nabla)\hat{s}) - \frac{1}{8\pi}\nabla B^2 \\ F &= (-1 + \hat{s}\hat{s}) \cdot \frac{\nabla B^2}{8\pi} + \frac{B^2}{4\pi}(\hat{s} \cdot \nabla)\hat{s}\end{aligned} \quad (2.4)$$

Consider $\frac{\nabla B^2}{8\pi}$ as a vector A, the first term on RHS of the above equation is

$$(-1 + \hat{s}\hat{s})A \implies -A + (\hat{s} \cdot A)\hat{s}$$

$(\hat{s} \cdot A)\hat{s}$ is the component of A parallel to \hat{s} i.e magnetic field and $A - (\hat{s} \cdot A)\hat{s} = -(-A + (\hat{s} \cdot A)\hat{s})$ is negative vector of the component of A perpendicular to magnetic field. Hence first term on the RHS of 2.4 represents the negative gradient of $\frac{B^2}{8\pi}$ in a direction perpendicular to magnetic field.

Finally, Lorentz force can be expressed as,

$$F = -\frac{\nabla_{\perp} B^2}{8\pi} + \frac{B^2}{4\pi} (\hat{s} \cdot \nabla) \hat{s} \quad (2.5)$$

2.3 Magnetic Tension and Pressure Forces

If a pressure function, p exists in a region then force density due to the pressure is expressed as $F = -\nabla p$. In equation 2.5, the first term on RHS represents a force density which is a gradient of $\frac{B^2}{8\pi}$. So, $\frac{B^2}{8\pi}$ is called the magnetic pressure force. It acts in a direction perpendicular to the magnetic field direction. In the second term on RHS of equation 2.5, $(\hat{s} \cdot \nabla) \hat{s}$ represents the curvature vector that points towards the center of curvature from a point on magnetic field [24].

$$(\hat{s} \cdot \nabla) \hat{s} = \frac{\hat{R}}{R_c}$$

Where R_c is the radius of curvature

$$F = -\frac{\nabla_{\perp} B^2}{8\pi} + \frac{B^2}{4\pi R_c} \hat{R} \quad (2.6)$$

The second term on the RHS of the above equation represents a force acting towards the centre of curvature, causing to straighten out curved magnetic fields. This is similar to tension in a string. Hence this force is called magnetic tension force.

Chapter 3

CME Dynamics

3.1 Effect of Lorentz force

First, we shall qualitatively see how Lorentz force could affect the dynamics of the CME flux rope

A confined plasma within magnetic fields would not have radial directed currents. Consider a cross-section of a CME as on Fig. 3.1, toroidal currents are running parallel to each other. As we know, parallel wires carrying current attract each other. So, a bundle of parallel running currents should come together leading to contraction of the cross-section of a CME. If we look at a CME from the top, we would observe Fig 3.2. As we can see the density of the magnetic field is higher on the inner side than the outer side. Such a configuration would lead to a force pointing radially away along the negative gradient of magnetic field density leading to an expansion of length of the CME.

Hence, we can conclude that Lorentz force would lead to,

- **Expansion** of length of CME
- **Contraction** of cross section of CME

Wang et al. (2009) [28] have concluded that Lorentz force leads to contraction of cross-section. This net effect of the Lorentz force is depicted in Fig. 3.3. But what we observe is that CMEs

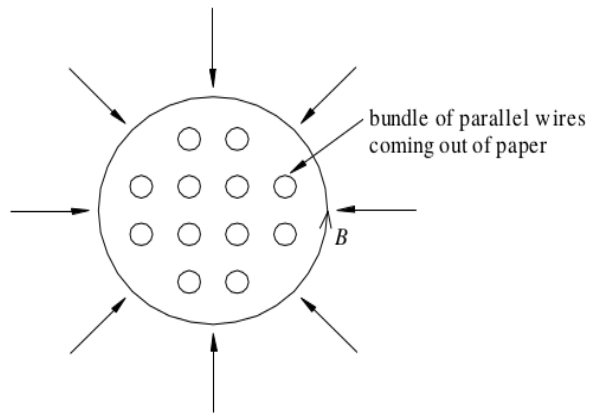


Figure 3.1: Parallel magnetic field lines in a cross-section of CME attract each other causing contraction

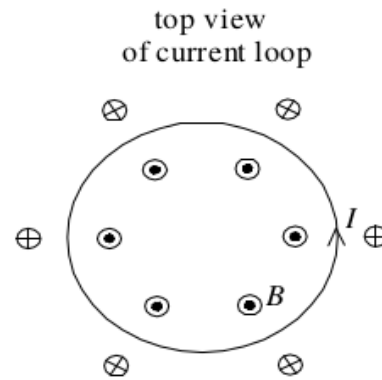


Figure 3.2: Top view of a CME torus from a distance (torus looks like a ring). Gradient in the magnetic field density causes expansion of length (major radius)

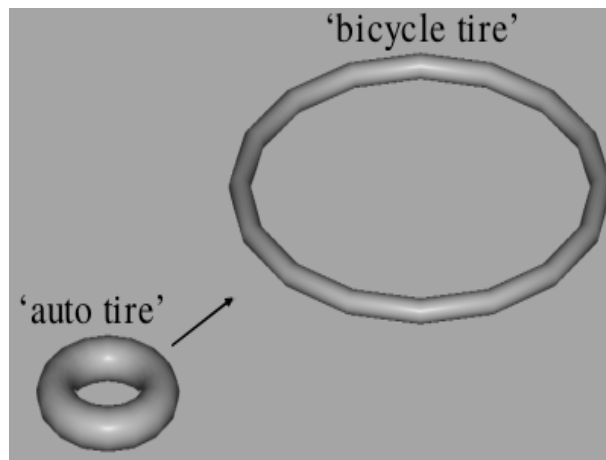


Figure 3.3: Net effect of Lorentz force on a CME torus. **Credits:** Fundamentals of plasma physics - Paul Bellan [2]

expand both in length and cross-section. This, along with the near earth temperatures of CMEs indicate plasma heating and increasing contribution of gas pressure as a CME expands

3.2 Major Radial Force Equation

Dynamics of a CME is in three dimensions. We would have three force equations. We shall assume self-similar expansion, which implies the cross section would expand symmetrically. So, we have two force equations along major and minor radii of a CME torus. First, we shall derive the major radial force equation. We shall assume that a CME is a complete torus and then divide the force expressions to get major and minor radial forces per unit length of CME.

3.2.1 Contribution of $J_t \times B_p$ force / Magnetic pressure force

The first term in Eq. 2.6 represents the major radial force density due to the gradient in magnetic pressure. In the case of CME torus, there is a gradient of poloidal field pressure (RHS of fig. ??). There is a force which arises due to the interaction of this non-uniform poloidal field with the toroidal current. This force density is acting **major radially outwards** (i.e. negative gradient of field). If we integrate this quantity over the volume, we get the corresponding force (called a hoop force, Miyamoto [18])

$$\int \left(\frac{\nabla_R B_p^2}{8\pi} \right) dV = \nabla_R \left(\int \frac{B_p^2}{8\pi} dV \right)$$

But the expression $\int \frac{B_p^2}{8\pi} dV$ is the magnetic energy stored in the poloidal fields, which can also be represented by $\frac{1}{2} L I_t^2$

So, the hoop force is given by,

$$\frac{d}{dR} \left(\frac{1}{2} L I_t^2 \right) = \frac{I_t^2}{2} \frac{d}{dR} (L)$$

Where, L, Inductance is given by, $L = \frac{4\pi R}{c^2} \left[\ln \left(\frac{8R}{a} \right) + \frac{\xi_i}{2} - 2 \right]$, where ξ_i represents the distribution of toroidal current across the cross section.

$$\frac{d}{dx}(\ln(ax)) = \frac{1}{x} \implies \frac{d}{dR}(L) = \frac{4\pi}{c^2} \left[\ln\left(\frac{8R}{a}\right) + \frac{\xi_i}{2} - 1 \right]$$

Hence, the hoop force is given by,

$$F_h = \frac{2\pi I_t^2}{c^2} \left[\ln\left(\frac{8R}{a}\right) + \frac{\xi_i}{2} - 1 \right] \hat{R} \quad (3.1)$$

3.2.2 Contribution of $J_p \times B_t$ force / Magnetic tension force

Now, we account for the tension force due to the curvature of the toroidal field which acts major radially inwards. This force arises due to the interaction of poloidal currents with the toroidal field. The radius of curvature for these toroidal field lines is R , major radius of the CME. From 2.6, we have tension force density acting towards the center of curvature i.e **major radially inwards** which is given by substituting $R_c = R$,

$$\frac{B_t^2}{4\pi R}$$

By integrating the above force density by volume we would have the force. And by assuming

$$\int (B_t^2) dV = \left(\frac{\overline{B_t^2}}{2}\right)V \implies \int \left(\frac{B_t^2}{4\pi R}\right) dV \approx \left(\frac{\overline{B_t^2}}{8\pi R}\right)V$$

Where $\overline{B_t^2}$ is the average over cross sectional area

$$\text{Volume of a CME, } V = 2\pi^2 a^2 R$$

Hence the tension force is given by,

$$F_t = - \left[\frac{\overline{B_t^2}}{8\pi} \right] 2\pi^2 a^2 \hat{R} \quad (3.2)$$

Myers et al. (2016) [20] have calculated the expression for this tension force by integrating $J_p \times B_t$ force density (Fig. 3.4) over volume and have shown this force per unit length is given by,

$$\frac{\pi a^2}{R} \left[\frac{\overline{B_t^2}}{8\pi} - \frac{B_{st}^2}{8\pi} \right]$$

Where B_{st} is the external toroidal field. But in our model, external field is poloidal i.e $B_{st} = 0$. So, the radially inward force due to toroidal tension is given by,

$$2\pi R \times \frac{\pi a^2}{R} \left[\frac{\overline{B_t^2}}{8\pi} \right] = 2\pi^2 a^2 \left[\frac{\overline{B_t^2}}{8\pi} \right]$$

Which is the same as eq. 3.2. So, the magnetic tension treatment is equivalent to $J_p \times B_t$ treatment

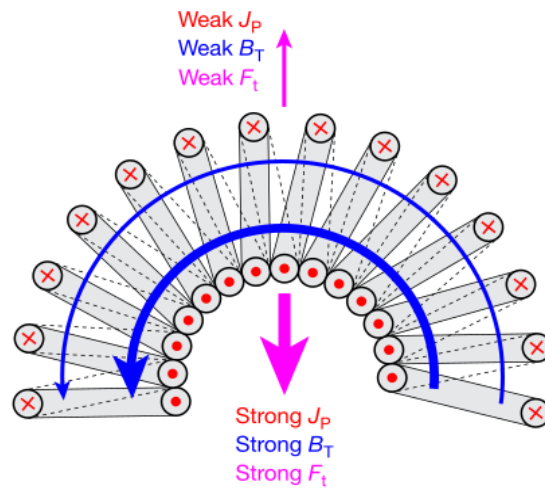


Figure 3.4: $J_p \times B_t$ force realised by Magnetic tension force

Credits: Myers et al. (2016) [20]

3.2.3 Contribution of pressure

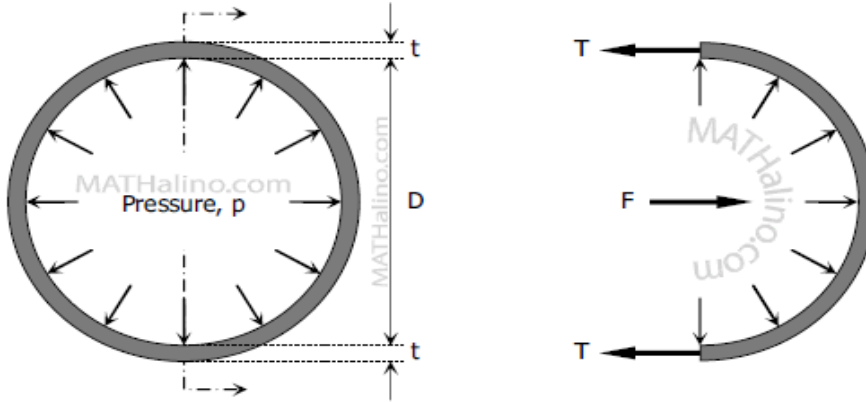


Figure 3.5: Relation between radial and tangential forces in cylindrical symmetry,
Credits: www.mathalino.com

Now, we have to account for the contribution of pressure towards major radial acceleration. Consider a hollow cylinder in LHS of fig. 3.5, where the length of the cylinder is L , and it is perpendicular to the plane of the paper. Let the major radial force be FR . We have

$$p = \frac{FR}{\pi DL}$$

Now consider the same hollow cylinder to be halved along a diameter as in RHS of fig. ??

$$F = pDL = 2T \implies p = \frac{2T}{DL}$$

$$\frac{FR}{\pi DL} = \frac{2T}{DL} \implies FR = 2\pi T, \text{ i.e Radial force} = 2\pi \times \text{Tangential force}$$

Our CME flux rope, when looked from top, has a similar cylindrical symmetry. In our case the tangential force, $T = (p - p_a) \times \pi a^2$.

Hence, force acting **major radially outwards** due to pressure is given by, $2\pi T$

$$F_p = (p - p_a) \times 2\pi^2 a^2 \hat{R} \quad (3.3)$$

3.2.4 Contribution of J_t and B_s (external magnetic field)

Finally, interaction of toroidal currents with external poloidal field gives rise to a force acting **major radially inward** ,

$$\frac{2\pi RB_s I_t}{c} = \frac{2I_t^2 \pi}{c^2} \left[\frac{2\pi RB_s I_t c^2}{2c I_t^2 \pi} \right] = \frac{2I_t^2 \pi}{c^2} \left[\frac{RB_s c}{I_t} \right]$$

Using again, $B_{pa} = \frac{2I_t}{ca}$

$$\frac{RB_s c}{I_t} = \frac{RB_s c}{I_t} \times \frac{B_{pa}}{B_{pa}} = \frac{RB_s c}{I_t} \times \frac{2I_t}{ca B_{pa}} = 2 \left(\frac{R}{a} \right) \left(\frac{B_s}{B_{pa}} \right)$$

Force due to external magnetic field is given by,

$$F_s = -2 \left(\frac{R}{a} \right) \left(\frac{B_s}{B_{pa}} \right) \hat{R} \quad (3.4)$$

The net Lorentz force acting along the major radial direction can be expressed by using equations 3.1 and 3.2,

$$F_L = F_h + F_t + F_s = \frac{2\pi I_t^2}{c^2} \left[\ln \left(\frac{8R}{a} \right) + \frac{\xi_i}{2} - 1 \right] - 2\pi^2 a^2 \left[\frac{\overline{B_t^2}}{8\pi} \right] - 2 \left(\frac{R}{a} \right) \left(\frac{B_s}{B_{pa}} \right) \hat{R}$$

In the above expression the first term dominates over the next two. **This is the force that we discussed qualitatively in the section 3.1 leading to CME length expansion.**

Now, consider the force due to pressure and toroidal tension together equations 3.3 and 3.2,

$$F_p + F_t = 2\pi^2 a^2 \left[p - p_a - \frac{\overline{B_t^2}}{8\pi} \right]$$

Now, taking $2 \times \frac{B_{pa}^2}{8\pi}$ common out of the brackets,

$$2\pi^2 a^2 \times 2 \times \frac{B_{pa}^2}{8\pi} \left[\frac{1}{2} \left(\frac{p - p_a}{B_{pa}^2/8\pi} \right) - \frac{1}{2} \frac{\overline{B_t^2}}{B_{pa}^2} \right] \quad (3.5)$$

Now, substituting, $B_{pa} = \frac{2I_t}{ca}$ the multiplying factor outside the brackets in the above equation

$$2\pi^2 a^2 \times 2 \times \frac{4I_t^2}{8\pi c^2 a^2} = \frac{2I_t^2 \pi}{c^2}$$

So, 3.5 now becomes, by using $\beta_p = \frac{p - p_a}{B_{pa}^2/8\pi}$

$$F_p + F_t = \frac{2I_t^2 \pi}{c^2} \left[\frac{\beta_p}{2} - \frac{1}{2} \frac{\overline{B_t^2}}{B_{pa}^2} \right] \hat{R} \quad (3.6)$$

Now using equations 3.4, 3.1 and 3.6 gives the major radial force expression,

$$F_L + F_p + F_s = \frac{2\pi I_t^2}{c^2} \left[\ln\left(\frac{8R}{a}\right) + \frac{\xi_i}{2} - 1 + \frac{\beta_p}{2} - \frac{1}{2} \frac{\overline{B_t^2}}{B_{pa}^2} - 2 \left(\frac{R}{a}\right) \left(\frac{B_s}{B_{pa}}\right) \right]$$

Now if we divide the above equation by $2\pi R$, we get the expression for major radial force per unit length

$$F_R = \frac{I_t^2}{c^2 R} \left[\ln\left(\frac{8R}{a}\right) + \frac{\xi_i}{2} - 1 + \frac{\beta_p}{2} - \frac{1}{2} \frac{\overline{B_t^2}}{B_{pa}^2} - 2 \left(\frac{R}{a}\right) \left(\frac{B_s}{B_{pa}}\right) \right] \hat{R} \quad (3.7)$$

In the above equation, the first three terms represent the contribution from $J_t \times B_p$ force. The next two terms represent the contribution from $J_p \times B_t$. The last term represents the $J_t \times B_s$ force.

3.3 Minor Radial Force Equation

3.3.1 Contribution of Tension force / $J_t \times B_p$ force

The tension force due to the curvature of poloidal field lines tends to contract cross-section of CME. From Eq. 2.6, using the expression for tension force density of poloidal field at the surface

using radius curvature, $R_c = a$, minor radius as,

$$\frac{B_{pa}^2}{4\pi a}$$

Now multiplying by volume, we have the tension force directed **minor radially outwards**

$$F_1 = -2\pi^2 a^2 R \left(\frac{B_{pa}^2}{4\pi a} \right) = -4\pi^2 a R \left[\frac{B_{pa}^2}{8\pi} \right] \hat{a} \quad (3.8)$$

3.3.2 Contribution of pressure

The **minor radially outward** directed force due to pressure can be straight forwardly expressed as

$$F_2 = \text{net pressure} \times \text{surface area of CME torus}$$

$$\text{Surface area of a torus} = (2\pi a)(2\pi R) = 4\pi^2 R a$$

$$F_2 = 4\pi^2 a R [p - p_a] \hat{a} \quad (3.9)$$

3.3.3 Contribution of Magnetic pressure gradient force / $J_p \times B_t$ force

As the external toroidal field is 0 in our model, there is a force due to the gradient of toroidal field acting **minor radially outwards**. Using the first term of eq. 2.6. This force density is given by,

$$\nabla_a \left(\frac{B_t^2}{8\pi} \right)$$

The force itself is given by,

$$F_3 = \nabla_a \left(\int \frac{B_t^2}{8\pi} dV \right) \approx \nabla_a \left(\frac{\overline{B_t^2}}{8\pi} \times 2\pi^2 a^2 R \right)$$

$$F_3 = \left(\frac{\overline{B_t^2}}{8\pi} \right) \times \nabla_a (2\pi^2 a^2 R)$$

$$F_3 = 4\pi^2 aR \left[\frac{\overline{B_t^2}}{8\pi} \right] \hat{a} \quad (3.10)$$

The net Lorentz force in the minor radial direction is given by,

$$F_L = F_1 + F_3 = -4\pi^2 aR \left[\frac{B_{pa}^2}{8\pi} - \frac{\overline{B_t^2}}{8\pi} \right] \hat{a}$$

for a confined plasma the first term would dominate the second and Lorentz force would lead to decrease in minor radius. **This is the force that we discussed qualitatively in the section, 3.1 to cause contraction of CME cross section.** However, In the force free approximation,

$$\frac{\overline{B_t^2}}{B_{pa}^2} = 1$$

Using equations 3.8, 3.9 and 3.10 we get the expression for the net minor radial force

$$F_1 + F_2 + F_3 = 4\pi^2 aR \left[\frac{\overline{B_t^2}}{8\pi} - \frac{B_{pa}^2}{8\pi} + p - p_a \right] \hat{a}$$

Now taking $\frac{B_{pa}^2}{8\pi}$ factor out of the brackets, and using $B_{pa} = \frac{2I_t}{ca}$ and invoking the formula of β_p , the minor radial force becomes

$$4\pi^2 aR \times \frac{4I_t^2}{8\pi c^2 a^2} \left[\frac{\overline{B_t^2}}{B_{pa}^2} - 1 + \beta_p \right] = \frac{2\pi R I_t^2}{c^2 a} \left[\frac{\overline{B_t^2}}{B_{pa}^2} - 1 + \beta_p \right]$$

Now, dividing the above expression by length of the CME, $2\pi R$ we get the minor radial force per unit length

$$F_a = \frac{I_t^2}{c^2 a} \left[\frac{\overline{B_t^2}}{B_{pa}^2} - 1 + \beta_p \right] \hat{a} \quad (3.11)$$

We can see that the major and minor radial force equations, 3.7 and 3.11 are the same equations in Chen, 1996 [6]

Chapter 4

Force-free Approximation

4.1 Motivation

We need information on the structure of field lines within the CMEs in our analysis. As the simplest solution, we consider force-free configuration for magnetic fields. In this configuration, the electromagnetic energy becomes minimum for a plasma with non-zero currents. Burlaga [5] has analyzed that the in-situ spacecraft observations of magnetic field profile as a CME passes by, roughly agrees with the fields represented by the force-free configuration. Further, it is fair to expect a system to evolve towards its minimum energy configuration.

We have estimated the magnetic field profile in this thesis in a later section 5.3. From our data, we had an estimate of the surface poloidal field only. By assuming force-free approximation, we were able to estimate average poloidal and toroidal fields and hence the net magnetic field of a CME as it evolved. Then we extrapolated these profiles to 1 AU and compared them with the observed field values at 1 AU. These extrapolated values agree very well with the observed values. These arguments indicate that the force-free approximation for the structure of magnetic fields is a reasonable one.

We assume the force-free configuration for fully formed CMEs as a first approximation, although it is not clear how CMEs would evolve into such a configuration. However, an exact force-free con-

figuration would make the Lorentz force vanish. Lorentz force plays a major role in the dynamics of CME, and we cannot allow them to vanish. However, a small angle between magnetic fields and currents would suffice to account for their contribution (Kumar and Rust [13]).

4.2 Force-free Configuration

For a plasma with non-zero currents, minimum energy occurs when,

$$\nabla \times B = \alpha B \quad (4.1)$$

We can show this by applying variation on electromagnetic energy of a plasma. The following analysis has been done by Spruit [24] In MHD approximation the induction equation relating magnetic and velocity fields is,

$$\frac{\partial B}{\partial t} = \nabla \times (v \times B)$$

For a small fluid displacement ξ ,

$$\delta B = \nabla \times (\xi \times B)$$

In MHD electric fields are neglected due to the infinite conductivity assumption. The net electromagnetic energy of plasma is given by,

$$E = \frac{1}{2\mu_o} \int B^2 dV$$

Now, inducing small displacements in a volume of plasma, energy change δE is given by ,

$$\begin{aligned} 2\mu_o \delta E &= \delta \left[\int B^2 dV \right] \\ \mu_o \delta E &= \int B \cdot \delta B dV = \int B \cdot \nabla \times (\xi \times B) dV \\ \mu_o \delta E &= \int (\nabla \times B) \cdot (\xi \times B) dV + \int [(\xi \times B) \times B] dS \end{aligned}$$

The surface term vanishes as the volume is kept constant

$$\mu_o \delta E = \int \xi \cdot [(\nabla \times B) \times B] dV$$

For δE to be minimum for an arbitrary ξ , we have

$$(\nabla \times B) \times B = 0 \implies \nabla \times B = \alpha B$$

Here α is a scalar function. It could be a constant. The configurations where the magnetic field satisfies 4.1 are called force free configurations and the fields are called force free.

4.3 Lundquist Solution

Now using 4.1, we have

$$\nabla \times (\nabla \times B) = \nabla \times (\alpha B) = \alpha^2 B$$

$$\nabla \times (\nabla \times B) = \nabla(\nabla \cdot B) - \nabla^2 B$$

But $\nabla \cdot B = 0$. Hence, we have ,

$$\nabla^2 B = -\alpha^2 B$$

The above equation is a Helmholtz equation for the magnetic field.

We model CMEs as a torus. The cross-section of a torus is cylindrically symmetrical. As a first approximation, the Helmholtz equation is solved under cylindrical symmetry, and we get the following solution called the force-free solution or Lundquist solution (Lundquist [17]).

$$B_t = B_o J_0(\alpha \mu_o r) \quad B_p = B_o J_1(\alpha \mu_o r) \quad B_r = 0$$

Here, B_p and B_t are the poloidal and toroidal magnetic fields, B_r is the minor radial field, α is the scalar function in Helmholtz equation, J_0 and J_1 are Bessel's functions of order 0 and 1. However, we have not considered the effect of the curvature of the torus itself on the structure of field lines and currents. The above solutions represent a family of helical magnetic fields embedded in the torus. The pitch angle (p.a, the angle between field direction and the axis of the cross-section) varying from 0 to 90 degrees. At the centre of this cross section(p.a=0°) the magnetic fields are only toroidal. At the surface of torus(p.a=90°), the magnetic field is only poloidal.

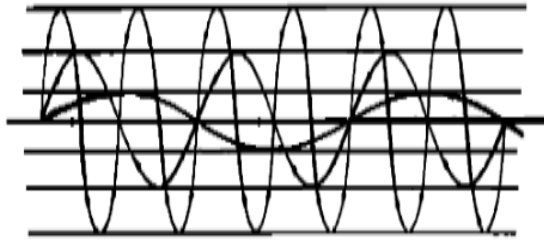


Figure 4.1: Force-free helical magnetic fields .
Credits: Burlaga, 1988



Figure 4.2: Force-free helical magnetic fields embedded in a CME torus
Credits: Burlaga, 1988

If we look a flux rope from a distance, $d \gg R$, we see a ring of current (Kumar and Rust[13]). Such a ring of current cannot produce a toroidal magnetic field immediately near its circumference. So, we take B_t to be zero at the boundary of the torus (at $r=a$). We have,

$$B_o J_o(\alpha \mu_o a) = 0 \implies \alpha \mu_o a = x_o$$

Here x_o is the first zero of the Bessel's function, $x_o = 2.405$

$$\alpha \mu_o r = \alpha \mu_o a \left(\frac{r}{a} \right) = x_o y$$

where y is the fractional minor radius The force free solution can be written as,

$$B_t = B_o J_o(x_o y) \quad B_p = B_o J_1(x_o y) \quad (4.2)$$

Chapter 5

Analysis

5.1 Data From GCS Fitting

A set of 38 well-observed, Earth-directed CMEs have been fitted with Graduated Cylindrical Shell model by Sachdeva et al. (2017) [23]. This model fits the visible CME shape with a 3-dimensional helical flux rope structure with tapering ends. Time profiles of height(h) of the leading edge and minor radius (a) have been obtained as parameters in the fitting.

We get the major radius (R) by,

$$R = h - a \quad (5.1)$$

which is true for a perfect torus.

The ratio of minor to major radius (termed as aspect ratio by Sachdeva et al.), κ is also evaluated. The value of this aspect ratio for all CMEs is given in 4th column of table 5.1

$$\kappa = \frac{a}{R} \quad (5.2)$$

Toroidal current, I_t has been obtained by assuming conservation of poloidal magnetic flux. I_t at equilibrium is estimated, where the Lorentz forces due to the magnetic fields inside the CME and the external magnetic field cancel each other (Kleim and Torok [12] equation).

$$I_{eq} = \frac{B_{eq}(h_{eq})h_{eq}c}{\ln\left(\frac{8h_{eq}}{a_{eq}}\right) - 2 + \frac{\xi_i}{2} + \frac{1}{2}}$$

I_{eq} values for all CMEs are in 6th column of table 5.1 and estimated $B_{eq}(h_{eq})$ values in 7th column of table 5.1.

Inductance of the CME at heliospheric distance, x is given by,

$$L_x = \frac{4\pi x}{c^2} \left[\ln\left(\frac{8x}{a_x}\right) - 2 + \frac{\xi_i}{2} \right]$$

Then the flux at equilibrium is equated with flux at arbitrary heliocentric distance (which is also the major radius, R) to get I_t as a function of heliocentric distance, R .

$$L_{eq}I_{eq} - \frac{1}{c} \int_0^{h_{eq}} B_s 2\pi r dr = L_R I_t(R) - \frac{1}{c} \int_0^R B_s 2\pi r dr$$

A model is assumed for external magnetic field

$$B_s = B_{eq}(h_{eq}) \frac{R^{-n}}{h_{eq}} \quad (5.3)$$

The value of n for each CME is given in 5th column of table 5.1

$$I_t(R) = \frac{c'_{eq} h_{eq} I_{eq}}{c' R} \left(1 + \frac{c'_{eq} + \frac{1}{2}}{2c'_{eq}(2-n)} \left[\left(\frac{R}{h_{eq}} \right)^{2-n} - 1 \right] \right) \quad (5.4)$$

where, where, $c'_{eq} = \ln\left(\frac{8h_{eq}}{a_{eq}}\right) - 2 + \frac{\xi_i}{2}$, $c' = \ln\left(\frac{8R}{a}\right) - 2 + \frac{\xi_i}{2}$

Hence, we have the profiles of minor and major radius (and hence κ), toroidal current and external magnetic field using GCS data and equations 5.1, 5.2, 5.3 and 5.4. Sachdeva et al. [23] have done the analysis mentioned in this section and have obtained data. The following table summarizes some parameters obtained for the 37 CMEs. The 3rd column gives the height of first observation. The 8th column gives the normaliation factor for Leblanc's model of solar wind density. The last column gives the mass estimate of each CME

No.	Date	h_o (R_{\odot})	κ	n	I_{eq} $10^{10}A$	$B_{ext}(h_{eq})$ $10^{-1}G$	n_{wind} cm^{-3}	Mass $10^{15}g$
1	2010 March 19	3.5	0.28	2.5	0.41	0.13	3.6	2.9
2	2010 April 3	5.5	0.34	1.6	3.13	0.94	7.1	5.85
3	2010 April 8	2.9	0.2	1.9	0.55	0.19	3.6	7.3
4	2010 June 16	5.7	0.23	2.5	0.31	0.11	3.5	2.3
5	2010 Sept 11	4	0.41	1.6	1.77	0.33	4	7.65
6	2010 October 26	5.3	0.25	1.7	0.66	0.22	3.8	7.14
7	2010 Dec 23	3.7	0.4	1.6	2.3	0.65	6.1	4.15
8	2011 January 24	4.4	0.3	1.6	1.21	0.38	9	7.86
9	2011 February 15	4.4	0.47	2.1	1.1	0.29	2.5	5.35
10	2011 March 3	4.9	0.35	2.5	0.5	0.15	2.25	3.13
11	2011 March 25	4.8	0.21	1.9	0.71	0.25	3	4.72
12	2011 April 8	4.7	0.3	2.5	0.47	0.15	5	5.61
13	2011 June 14	3.6	0.26	1.6	1.72	0.56	3.7	10.3
14	2011 June 21	8.4	0.45	1.6	6.26	1.71	8	4.98
16	2011 August 4	7.3	0.69	1.6	5.9	1.39	2	6.17
17	2011 Sept 13	3.8	0.43	1.7	1.06	0.29	2.13	4.87
18	2011 October 22	4	0.6	2.1	8.4	2.09	8	1.31
19	2011 October 26	7.8	0.46	2.1	0.47	0.13	3	3.61
20	2011 October 27	5.3	0.36	2.2	1.67	0.49	8.42	3.01
21	2012 January 19	4.6	0.47	3	11.6	3.11	7	9.17
22	2012 January 23	4	0.48	3	10.3	2.74	6	14.76
23	2012 January 27	3.5	0.38	3	8.51	2.47	4	12.45
24	2012 March 13	3.9	0.74	1.9	3.92	0.91	1	10.04
25	2012 April 19	4.1	0.27	1.6	3.68	1.19	10	5.93
26	2012 June 14	6.2	0.38	1.6	2.89	0.84	3.23	5.65
27	2012 July 12	4.4	0.45	1.6	4.07	1.11	3.2	14.8
28	2012 Sep 28	6.7	0.42	1.6	8.53	2.37	7	8.96
29	2012 October 5	4.4	0.3	1.6	4.05	1.28	6	6.72
30	2012 October 27	7.3	0.2	1.6	1.56	0.56	5	3.7
31	2012 November 9	3.8	0.48	2.9	11.07	2.96	13	5.19
32	2012 Nov 23	6.3	0.52	1.7	3.41	0.89	7	3.45
33	2013 March 15	4.7	0.31	1.8	4.29	1.32	4.5	1.74
34	2013 April 11	5.9	0.14	1.6	1.29	0.52	3.3	15.1
35	2013 June 28	6.6	0.41	2.5	9.55	2.69	10	3.33
36	2013 Sep 29	4.9	0.38	2.1	7.06	2.04	11	13.73
37	2013 November 7	5.9	0.34	1.7	2.5	0.75	5.5	5.25
38	2013 December 7	6.8	0.36	1.9	6.91	2.04	15	4.87

Table 5.1: CME parameters

5.2 Estimation of Expressions of β_p , Pressure and Temperature

5.2.1 β_p

This is the main part of my work. I have analysed 37 of the 38 CMEs (except for CME 15) which have been studied by Sachdeva et al. We use the major and minor radial force equations to estimate physical quantities of a CME which are temperature, pressure and plasma beta. The equations are as follows,

$$F_R = \frac{I_t^2}{c^2 R} \left[\ln\left(\frac{8R}{a}\right) + \frac{\beta_p}{2} - \frac{1}{2} \frac{\overline{B_t^2}}{B_{pa}^2} - 2\left(\frac{R}{a}\right) \frac{B_s}{B_{pa}} - 1 + \frac{\xi_i}{2} \right] + F_d, \quad (5.5)$$

$$F_a = \frac{I_t^2}{c^2 a} \left[\frac{\overline{B_t^2}}{B_{pa}^2} - 1 + \beta_p \right] \quad (5.6)$$

We neglect aerodynamic drag. We have F_R and F_a which are major and minor radial forces per unit length.

$$F_R = m \frac{d^2 R}{dt^2} \qquad F_a = m \frac{d^2 a}{dt^2}$$

Here, m is the mass of the CME per unit length.

From the GCS data, we can observe that the **ratio of minor radius to the major radius of a CME roughly remains constant as the CME evolves** for all the CMEs we investigate. We assume that this ratio, κ is constant for a CME. So,

$$\frac{a}{R} = \kappa = \frac{d^2 a}{dt^2} \bigg/ \frac{d^2 R}{dt^2} = \frac{F_a}{F_R}$$

$$\implies \kappa F_R = F_a$$

Substituting expressions of F_R and F_a , we have

$$\kappa \frac{I_t^2}{c^2 R} \left[\ln\left(\frac{8R}{a}\right) + \frac{\beta_p}{2} - \frac{1}{2} \frac{\overline{B_t^2}}{B_{pa}^2} - 2\left(\frac{R}{a}\right) \frac{B_s}{B_{pa}} - 1 + \frac{\xi_i}{2} \right] = \frac{I_t^2}{c^2 a} \left[\frac{\overline{B_t^2}}{B_{pa}^2} - 1 + \beta_p \right]$$

Cancelling $\frac{I_t^2}{c^2}$ on both sides and again using $\kappa = \frac{a}{R}$

$$\kappa^2 \left[\ln\left(\frac{8}{\kappa}\right) + \frac{\beta_p}{2} - \frac{1}{2} \frac{\overline{B}_t^2}{B_{pa}^2} - 2\left(\frac{R}{a}\right) \frac{B_s}{B_{pa}} - 1 + \frac{\xi_i}{2} \right] = \left[\frac{\overline{B}_t^2}{B_{pa}^2} - 1 + \beta_p \right]$$

$$\left[\ln\left(\frac{8}{\kappa}\right) + \frac{\beta_p}{2} - \frac{1}{2} \frac{\overline{B}_t^2}{B_{pa}^2} - 2\left(\frac{R}{a}\right) \frac{B_s}{B_{pa}} - 1 + \frac{\xi_i}{2} \right] = \left[\frac{1}{\kappa^2} \left(\frac{\overline{B}_t^2}{B_{pa}^2} \right) - \frac{1}{\kappa^2} + \left(\frac{1}{\kappa^2} \right) \beta_p \right]$$

For force free fields, $\xi = 1$ (Subramanian et al. 2009 [26])

Taking all β_p terms to RHS

$$\left[\ln\left(\frac{8}{\kappa}\right) - \frac{1}{2} \frac{\overline{B}_t^2}{B_{pa}^2} - \frac{1}{\kappa^2} \left(\frac{\overline{B}_t^2}{B_{pa}^2} \right) - 2\left(\frac{R}{a}\right) \frac{B_s}{B_{pa}} - 1 + \frac{1}{2} + \frac{1}{\kappa^2} \right] = \left[\left(\frac{1}{\kappa^2} \right) \beta_p - \frac{\beta_p}{2} \right]$$

$$\left[\ln\left(\frac{8}{\kappa}\right) - \frac{\overline{B}_t^2}{B_{pa}^2} \left(\frac{1}{2} + \frac{1}{\kappa^2} \right) - 2\left(\frac{R}{a}\right) \frac{B_s}{B_{pa}} + \frac{1}{\kappa^2} - \frac{1}{2} \right] = \beta_p \left(\frac{1}{\kappa^2} - \frac{1}{2} \right)$$

$$\beta_p = \frac{2\kappa^2}{2 - \kappa^2} \left[\ln\left(\frac{8}{\kappa}\right) - \frac{\overline{B}_t^2}{B_{pa}^2} \left(\frac{2 + \kappa^2}{2\kappa^2} \right) - 2\left(\frac{R}{a}\right) \frac{B_s}{B_{pa}} + \frac{2 - \kappa^2}{2\kappa^2} \right]$$

We shall assume a uniform toroidal current density to get a relationship between I_t and B_p . Using Ampere's law in cgs units

$$\oint B \cdot dl = \frac{4\pi}{c} I_{enc} \implies B_{pa}(2\pi a) = \frac{4\pi}{c} I_t$$

$$B_{pa} = \frac{2I_t}{ca} \quad (5.7)$$

Using the above expression for B_{pa} in the third term on RHS, expression for β_p becomes,

$$\beta_p = \frac{2\kappa^2}{2 - \kappa^2} \left[\ln\left(\frac{8}{\kappa}\right) - \frac{\overline{B}_t^2}{B_{pa}^2} \left(\frac{2 + \kappa^2}{2\kappa^2} \right) - 2\left(\frac{R}{a}\right) \frac{B_s ca}{2I_t} \right] + 1$$

$$\beta_p = \frac{2\kappa^2}{2 - \kappa^2} \left[\ln\left(\frac{8}{\kappa}\right) - \frac{\overline{B}_t^2}{B_{pa}^2} \left(\frac{2 + \kappa^2}{2\kappa^2} \right) - \frac{B_s cR}{I_t} \right] + 1 \quad (5.8)$$

Using, $\beta_p = \frac{8\pi(\bar{p} - p_a)}{B_{pa}^2}$,

$$\frac{8\pi(\bar{p})}{B_{pa}^2} = \beta_p + \frac{8\pi(p_a)}{B_{pa}^2}$$

$$\text{Plasma Beta} = \beta_p + \frac{8\pi(p_a)}{B_{pa}^2} \quad (5.9)$$

5.2.2 Pressure

By the definition of β_p in Chen, 1996 [6], we have

$$\beta_p = \frac{8\pi(\bar{p} - p_a)}{B_{pa}^2}$$

Now, we consider the average pressure, \bar{p} an the pressure of the CME, and using eq. 5.7

$$\bar{p} = \frac{\beta_p B_{pa}^2}{8\pi} + p_a$$

$$p = \frac{I_t^2 \beta_p}{2\pi c^2 a^2} + p_a \quad (5.10)$$

$$p = \frac{I_t^2 \kappa^2}{\pi c^2 a^2 (2 - \kappa^2)} \left[\ln\left(\frac{8}{\kappa}\right) - \frac{\bar{B}_t^2}{B_{pa}^2} \left(\frac{2 + \kappa^2}{2\kappa^2}\right) - \frac{B_{sc} R}{I_t} + \frac{2 - \kappa^2}{2\kappa^2} \right] + p_a \quad (5.11)$$

5.2.3 Temperature

If we write an ideal gas equation for the plasma, it would be,

$$p = n_p k_b T_p + n_e k_b T_e$$

Where n_e and n_p are the number densities of electrons and protons. We assume that plasma is made only from hydrogen. So, $n_e = n_p = n$. We also assume that both protons and electrons are in thermal equilibrium with each other at the same temperature, T.

$$p = 2nk_b T \implies T = \frac{p}{2nk_b} \quad (5.12)$$

$$T = \frac{1}{2nk_b} \left[\frac{I_t^2 \kappa^2}{\pi c^2 a^2 (2 - \kappa^2)} \left[\ln\left(\frac{8}{\kappa}\right) - \frac{\overline{B_t^2}}{B_{pa}^2} \left(\frac{2 + \kappa^2}{2\kappa^2} \right) - \frac{B_s c R}{I_t} + \frac{2 - \kappa^2}{2\kappa^2} \right] + p_a \right] \quad (5.13)$$

We assume that half of the CME toroid is submerged in the photosphere. So, Volume of CME (V) = length of CME \times cross-sectional area of CME

$$V = (\pi a^2)(\pi R) = \pi^2 a^2 R$$

If M is the total mass of the CME and m_p is the mass of proton, then the number density of CME assuming it is made up of hydrogen,

$$n = \frac{\text{density}}{\text{mass of proton}} = \frac{M}{V m_p} = \frac{M}{m_p \pi^2 a^2 R}$$

Using the above expression in 5.13

$$T = \frac{\pi^2 a^2 R m_p}{2M k_b} \left[\frac{I_t^2 \kappa^2}{\pi c^2 a^2 (2 - \kappa^2)} \left[\ln\left(\frac{8}{\kappa}\right) - \frac{\overline{B_t^2}}{B_{pa}^2} \left(\frac{2 + \kappa^2}{2\kappa^2} \right) - \frac{B_s c R}{I_t} + \frac{2 - \kappa^2}{2\kappa^2} \right] + p_a \right] \quad (5.14)$$

5.2.4 Evaluating $\frac{\overline{B_t^2}}{B_{pa}^2}$ using force-free solutions

In the above expression, $\frac{\overline{B_t^2}}{B_{pa}^2}$ is evaluated using force-free solution 4.2. The average of a quantity, x is defined by Chen, 1996 [6] as,

$$\bar{x} = \frac{2}{a^2} \int_0^a r x dr = 2 \int_0^1 y x dy \quad (5.15)$$

where $y = \frac{r}{a}$ is the fractional minor radius.

The above expression actually gives the average over cross-sectional area of the CME. We shall check that

$$\bar{x} = \frac{\text{integral of x over cross-section}}{\text{cross-sectional area}} = \frac{\int_0^a x 2\pi r dr}{\pi a^2} = \frac{2\pi \int_0^a r x dr}{\pi a^2} = \frac{2}{a^2} \int_0^a r x dr$$

$$\overline{B_t} = \frac{2}{a^2} \int_0^a r B_t dr = 2 \int_0^1 y B_t dy$$

B_{pa} is the poloidal field at surface of CME i.e at $r = a$ or $y=1$.

$$B_p = B_o J_1(x_o y) \implies B_{pa} = B_o J_1(x_o) \quad (5.16)$$

$$\frac{\overline{B_r^2}}{B_{pa}^2} = 4 \left[\frac{\int_0^1 y J_o(x_o y) dy}{J_1(x_o)} \right]^2$$

$x_0 = 2.405$, is the first zero of Bessel's function J_0 .

I calculated the value of above expression using mathematica to be 1 with precision upto 4th decimal place.

5.2.5 Pressure of the ambient solar wind

We evaluate the pressure of the ambient solar wind, p_a values using models. First, we estimate the solar wind density using the model by Leblanc et al. (1998) [14]

$$n_a(R) = \left(\frac{n_{wind}}{7.2} \right) \left[3.3 \times 10^5 R^{-2} + 4.1 \times 10^6 R^{-4} + 8 \times 10^7 R^{-6} \right] cm^{-3}$$

where, R is the heliocentric distance of the CME in solar radii. In the above expression, the expression within square brackets is the estimate given by Leblanc assuming that the number density at 1 AU is always same, i.e $7.2 cm^{-3}$. The factor $\left(\frac{n_{wind}}{7.2} \right)$ normalizes the original expression such that the number density matches the value observed through WIND space craft during these CME events. We can find n_{wind} values in Sachdeva et al. (2017) [23] The temperature of solar wind as a function of heliocentric distance is given by Venzmer and Bothmer [27],

$$T_a = 1.654 \left(197 \times ssn + 57300 \right) r^{-1.1} K$$

where r is measured in AU $\left(r = \frac{R}{215} \right)$ and ssn is the sunspot number on the day CME was observed. It can be obtained from the website with URL <http://www.sidc.be/silso/datafiles>. The gas equation of solar wind would be

$$p_a = 2n_a k_b T_a$$

$$p_a = \left[n_{wind} \times 0.00125 \times k_b \left(3.3 \times 10^5 R^{-2} + 4.1 \times 10^6 R^{-4} + 8 \times 10^7 R^{-6} \right) \left(197 \times ssn + 57300 \right) R^{-1.1} \right] dynes$$

5.3 Estimation of Magnetic Field Profile

We have an estimate of surface poloidal field, B_{pa} as a function of heliocentric distance as

$$B_{pa} = \frac{2I_t}{ca}$$

Using eq. 5.16 ,

$$B_{pa} = B_o J_1(2.405y)$$

Equating the above two expressions, value of B_o can be found out. Now, we can find the magnitudes of average poloidal and toroidal field by using equations 5.15 and 4.2

$$\overline{B_p} = 2 \int_0^1 B_o J_1(2.405y) y dy$$

$$\overline{B_t} = 2 \int_0^1 B_o J_o(2.405y) y dy$$

The magnitude of net magnetic field is given by,

$$B_{net} = \sqrt{\overline{B_p}^2 + \overline{B_t}^2} \quad (5.17)$$

We also have B values at 1 AU. We can extrapolate the profile obtained by data to 1 AU and compare it with the observed value.

To extrapolate the B value, first I removed initial range of data points, where B falls deeply. I used cubic spline interpolation on the to extrapolate B value at 1 AU. But this method would be effective, if we have data almost upto 1 AU for all CMEs which is not the case.

This is because the slope of the interpolated curve would change signs before reaching 1 AU and giving very off results. So, I have fit the profile with the functions of the form $a(b^{cx}) + d$ and $a(x^b)$, where a,b,c,d are parameters and then extrapolated the function to 1 AU. The least percentage RMS error occurred for the fitting of $a(x^b)$ function. So, I have calculated error in B values using this fit

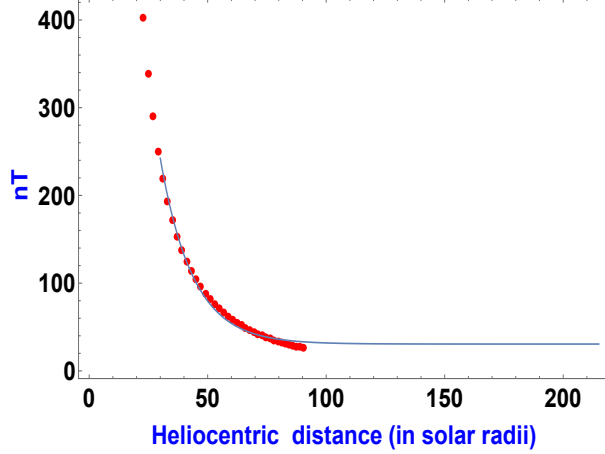


Figure 5.1: Extrapolation by fitting $a(b^{cx}) + d$

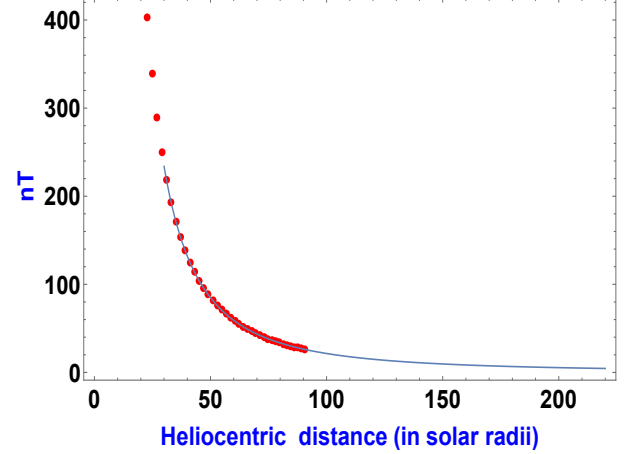


Figure 5.2: Extrapolation by fitting $a(x^b)$

5.4 Inconsistencies due to differences in two models: Torus Instability Model (Kleim and Torok) and Flux Injection Model (Chen)

5.4.1 Sign of the term representing the effect of external magnetic field

In the GCS fitting, Torus Instability (TI) model by Kleim and Torok [12] has been used to estimate I_t . We use flux injection model suggested by Chen in our analysis.

The major radial force per unit length in the TI model is given by,

$$F_R = \frac{I^2}{c^2 R} \left[\ln\left(\frac{8R}{a}\right) - \frac{3}{2} + \frac{\xi_i}{2} \right] - \frac{B_s I}{c} \quad (5.18)$$

Where, the last term $\frac{B_s I}{c}$ is the force due to external poloidal magnetic field which opposes the major radial expansion. Here I is the plasma current, which is toroidal and is analogous to I_t in Chen's (1996) [6] model.

The major radial force per unit length is given in Chen's model by

$$F_R = \frac{I_t^2}{c^2 R} \left[\ln\left(\frac{8R}{a}\right) + \frac{\beta_p}{2} - \frac{1}{2} \frac{\overline{B_t^2}}{B_{pa}^2} + 2 \left(\frac{R}{a}\right) \frac{B_s}{B_{pa}} - 1 + \frac{\xi_i}{2} \right] \quad (5.19)$$

The fourth term in the above equation expresses the contribution from external poloidal magnetic field. Substituting $B_{pa} = \frac{2I_t}{ca}$ and taking it out of the brackets, the term becomes

$$\frac{I_t^2}{c^2 R} \left[2 \left(\frac{R}{a} \right) \frac{B_s ca}{2I_t} \right] = \frac{B_s I_t}{c}$$

But this term has a positive sign in the major radial force equation as compared to the negative sign in the Kleim and Torok model. However, in Chen's model the relation between B_s and B_{pa} at equilibrium is as follows,

$$B_{so} = -\frac{a_o}{2R_o}$$

and external field is modelled by,

$$B_s(Z) = B_{so} \text{sech}^2 \left(\frac{|z - z'|}{h} \right)$$

So, B_s is always opposite to B_{pa} and $\frac{B_s}{B_{pa}}$ is always negative in Chen's model. Since we have used the B_s values estimated using Kleim and Torok model, we change the sign of the term, $\frac{B_s I_t}{c}$ in Chen's equation in our analysis. Hence, the Chen equation becomes,

$$F_R = \frac{I_t^2}{c^2 R} \left[\ln \left(\frac{8R}{a} \right) + \frac{\beta_p}{2} - \frac{1}{2} \frac{\overline{B_t^2}}{B_{pa}^2} - 1 + \frac{\xi_i}{2} \right] - \frac{B_s I_t}{c}$$

5.4.2 Role of pressure in the two models

The minor radial force per unit length which causes CME cross section expansion is given in the Chen model by,

$$F_a = \frac{I_t^2}{c^2 a} \left[\frac{\overline{B_t^2}}{B_{pa}^2} - 1 + \beta_p \right]$$

Now neglecting the effects of plasma beta ($\beta_p=0$) in these equations, we have,

$$F_R = \frac{I_t^2}{c^2 R} \left[\ln \left(\frac{8R}{a} \right) - \frac{1}{2} \frac{\overline{B_t^2}}{B_{pa}^2} - 1 + \frac{\xi_i}{2} \right] - \frac{B_s I_t}{c} \quad (5.20)$$

$$F_a = \frac{I_t^2}{c^2 a} \left[\frac{\overline{B_t^2}}{B_{pa}^2} - 1 \right]$$

But this minor radial expansion is neglected in TI model, where minor radial force is equated to 0. Then we have

$$\frac{\overline{B_t^2}}{B_{pa}^2} - 1 = 0 \implies -\frac{1}{2} \frac{\overline{B_t^2}}{B_{pa}^2} = -\frac{1}{2}$$

Substituting this in 5.20, we have

$$F_R = \frac{I_t^2}{c^2 R} \left[\ln\left(\frac{8R}{a}\right) - \frac{1}{2} + -1 + \frac{\xi_i}{2} \right] - \frac{B_s I_t}{c}$$

$$F_R = \frac{I_t^2}{c^2 R} \left[\ln\left(\frac{8R}{a}\right) - \frac{3}{2} + \frac{\xi_i}{2} \right] - \frac{B_s I_t}{c}$$

This is the Kleim Torok Equation. So, we can go from Chen's equation to Kleim and Torok equation by neglecting the pressure contribution towards CME dynamics and minor radial expansion. Summarizing the above arguments, we have fit CMEs using TI model which neglects cross-section expansion and contribution of gas pressure to estimate plasma current (I). But this current has been used by us as I_t in Chen's model to investigate the contribution of gas pressure and expansion of cross-section. There is an inconsistency here.

5.4.3 Over-estimation of I_t

Equating the force expressions in the two models, we get a relation between I and I_t

$$\frac{I^2}{c^2 R} \left[\ln\left(\frac{8R}{a}\right) - \frac{3}{2} + \frac{\xi_i}{2} \right] - \frac{B_s I}{c} = \frac{I_t^2}{c^2 R} \left[\ln\left(\frac{8R}{a}\right) + \frac{\beta_p}{2} - \frac{1}{2} \frac{\overline{B_t^2}}{B_{pa}^2} - 1 + \frac{\xi_i}{2} \right] - \frac{B_s I_t}{c}$$

Considering that both the terms $\frac{B_s I}{c}$ and $\frac{B_s I_t}{c}$ represent the same force due to external magnetic

field on toroidal current, we can cancel them on both sides

$$I_t^2 = I^2 \frac{\left[\ln\left(\frac{8R}{a}\right) - \frac{3}{2} + \frac{\xi_i}{2} \right]}{\left[\ln\left(\frac{8R}{a}\right) + \frac{\beta_p}{2} - \frac{1}{2} \frac{\overline{B_t^2}}{B_{pa}^2} - 1 + \frac{\xi_i}{2} \right]}$$

Now, using the force free solutions, we have $\xi = 1$ and $\frac{1}{2} \frac{\overline{B_t^2}}{B_{pa}^2} = \frac{1}{2} = 0.5$

$$I_t^2 = I^2 \frac{\left[\ln\left(\frac{8R}{a}\right) - 1 \right]}{\left[\ln\left(\frac{8R}{a}\right) + \frac{\beta_p}{2} - 1 \right]}$$

$$I_t = I \sqrt{\frac{\ln\left(\frac{8R}{a}\right) - 1}{\ln\left(\frac{8R}{a}\right) + \frac{\beta_p}{2} - 1}} \quad (5.21)$$

So, numerator is always smaller than denominator

$$I_t < I$$

I_t is overestimated by using I .

The expression of plasma beta 5.8 is,

$$\beta_p = \frac{2\kappa^2}{2 - \kappa^2} \left[\ln\left(\frac{8}{\kappa}\right) - \frac{\overline{B_t^2}}{B_{pa}^2} \left(\frac{2 + \kappa^2}{2\kappa^2} \right) - \frac{B_s c R}{I_t} \right] + 1$$

This overestimation of I_t is realized in β_p values through the third term in the above equation. Hence β_p is also overestimated.

$$\beta_p(\text{Estimated}) > \beta_p(\text{Actual})$$

$$p(\text{Estimated}) > p(\text{Actual})$$

Also, since temperature is proportional to β_p ,

$$T(\text{Estimated}) > T(\text{Actual})$$

Out of all the terms within the square brackets in the above equation, third term is an order of magnitude lesser than the other two terms So, this overestimation in plasma beta would be very small.

5.4.4 Error due to over estimation of I_t

We can estimate error in pressure and temperature due to over estimation in I_t . Using 5.21,

$$I_t = I \sqrt{\frac{\ln\left(\frac{8R}{a}\right) - 1}{\ln\left(\frac{8R}{a}\right) + \frac{\beta_p}{2} - 1}}$$

Let,

$$\frac{\ln\left(\frac{8R}{a}\right) - 1}{\ln\left(\frac{8R}{a}\right) + \frac{\beta_p}{2} - 1} = A$$

We can observe from the GCS fitting data that,

$$2.38 \leq \ln\left(\frac{8R}{a}\right) \leq 4.07$$

$$0.44 \leq \beta_p \leq 1.8 \implies 0.22 \leq \frac{\beta_p}{2} \leq 0.9$$

Minimum value of A, occurs for $\ln\left(\frac{8R}{a}\right) = 2.38$ and $\frac{\beta_p}{2} = 0.9$

$$\min(A) = \sqrt{\frac{2.38 - 1}{2.38 + 0.9 - 0.845}} = 0.77$$

Maximum error occurs at min A, max error = $\frac{I - I_t}{I_t} \times 100 = 29.8\%$

Maximum value of A, occurs for $\ln\left(\frac{8R}{a}\right) = 4.7$ and $\frac{\beta_p}{2} = 0.22$

$$\max(A) = \sqrt{\frac{4.7 - 1}{4.7 + 0.22 - 0.845}} = 0.97$$

Minimum error occurs at max A, min error = 3.1 %

Hence, the error due to over estimation of I_t is in between 3.1 % and 29.8 %

5.5 Estimation of Polytropic Index and Heating Rates

Assuming that expansion of a CME is a polytropic process.

Assuming a polytropic relation for the system, $PV^n = P\rho^{-n} = \text{constant} = C$

$$\ln(p) = n \ln(\rho) + \text{constant} \quad (5.22)$$

We can estimate polytropic index as the slope of graph between $\ln(p)$ vs $\ln(\rho)$ When the CME system goes from P_1, V_1, T_1 to P_2, V_2, T_2

$$C = P_1 V_1^n = P_2 V_2^n \quad (5.23)$$

Work done is given by

$$\Delta W = \int_1^2 P dV = \int_1^2 C V^{-n} dV = \int_1^2 \frac{C V^{1-n}}{1-n}$$

$$\Delta W = \frac{1}{1-n} (C V_2^{1-n} - C V_1^{1-n})$$

Using 5.23, we have

$$\Delta W = \frac{(P_2 V_2 - P_1 V_1)}{1-n} = \frac{(P_1 V_1 - P_2 V_2)}{n-1}$$

Using $PV = mRT$, we have

$$\Delta W = \frac{mR(T_1 - T_2)}{n-1}$$

Internal energy change is given by its definition, heat exchanged at constant volume

$$\Delta U = mC_v(T_2 - T_1)$$

$$\Delta U = -mC_v(T_1 - T_2)$$

Where, C_v , specific heat capacity at constant volume

$$C_p - C_v = R \implies \frac{C_p}{C_v} - 1 = \frac{R}{C_v}$$

$$\gamma - 1 = \frac{R}{C_v} \implies C_v = \frac{R}{\gamma - 1}$$

Here γ is the adiabatic index. Using the above expression for C_v , we have

$$\Delta U = \frac{-mR(T_1 - T_2)}{\gamma - 1}$$

First law of thermodynamics states,

$$\Delta Q = \Delta U + \Delta W$$

Using expressions for ΔW and ΔU

$$\Delta Q = \frac{-mR(T_1 - T_2)}{\gamma - 1} + \frac{mR(T_1 - T_2)}{n - 1}$$

$$\Delta Q = mR(T_1 - T_2) \left[\frac{1}{n - 1} - \frac{1}{\gamma - 1} \right]$$

$$\Delta Q = \frac{mR(T_1 - T_2)(\gamma - n)}{(\gamma - 1)(n - 1)} \quad (5.24)$$

We could estimate heating budget between every two data points. We also have time as a function of heliocentric distance So, we could get an estimate of heating rates between pairs of adjacent data points and we can evaluate profiles of heating budgets and rates.

$$\text{Heating Rate} = \frac{\Delta Q}{\Delta t} = \frac{mR(T_1 - T_2)(\gamma - n)}{(\gamma - 1)(n - 1)(\Delta t)} \quad (5.25)$$

5.6 Estimation of CME Temperature at 1 AU for an Adiabatic Expansion

I tried to get a crude estimate of the temperature of CMEs at 1 AU if they were to expand adiabatically. If CMEs expanded adiabatically,

$$PV^\gamma = \text{constant} \implies TV^{\gamma-1} = \text{constant}$$

Volume of CME is given by, $V = \pi^2 a^2 R$

$$R = \frac{a}{\kappa} \implies V = \frac{\pi^2 a^3}{\kappa} \quad (5.26)$$

For an adiabatically expanding CME, we have

$$T_o V_o^{\gamma-1} = T_f V_f^{\gamma-1}$$

Where T_o and V_o are temperature and volume at equilibrium, before CME starts expanding. T_f and V_f are the values at 1 AU.

$$T_f = T_o \left(\frac{V_o}{V_f} \right)^{\gamma-1}$$

Using Equation 5.26, we have

$$T_f = T_o \left(\frac{a_o^3}{a_f^3} \right)^{\gamma-1}$$

Since, we assume that CME is mostly made of hydrogen, $\gamma = \frac{5}{3}$

$$T_f = T_o \left(\frac{a_o^3}{a_f^3} \right)^{5/3-1} \implies T_f = T_o \left(\frac{a_o}{a_f} \right)^2$$

Chen (1996) [6] have estimated a_0 to be of the order 10^5 km and T_o to about 10^6 K. The GCS fitting data is available for CME 2 until 210 solar radii which is of the order 10^8 km.

$$T_f = 2 \times 10^6 \left(\frac{10^5}{10^8} \right)^2 = 2K$$

This is in good agreement with the temperature estimated by Chen and Garren (1993) [10] which is 3 kelvin This estimate shows that the temperature at 1 AU would be about a few degrees of kelvin.

Chapter 6

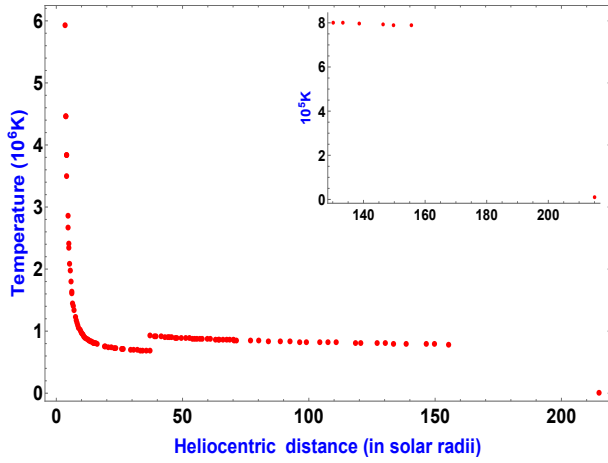
Results and Discussions

Using the expressions for β_p , plasma beta, pressure, temperature from equations 5.8, 5.9, 5.11, 5.14 and 5.25, we can get profiles of the respective quantities as the CME evolves for the 38 CMEs we have analyzed. I have presented representative profiles of 6 CMEs. In all the following plots, x- axis is the heliocentric distance of the apex of the CME.

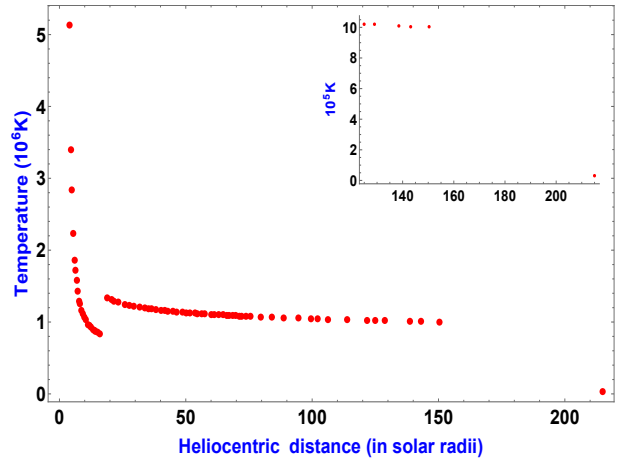
6.1 Temperature Profiles

We also have temperature values at 1 AU from WIND spacecraft. We have plotted that too along with evaluated profiles to investigate the amount of temperature change between last data point and 1 AU.

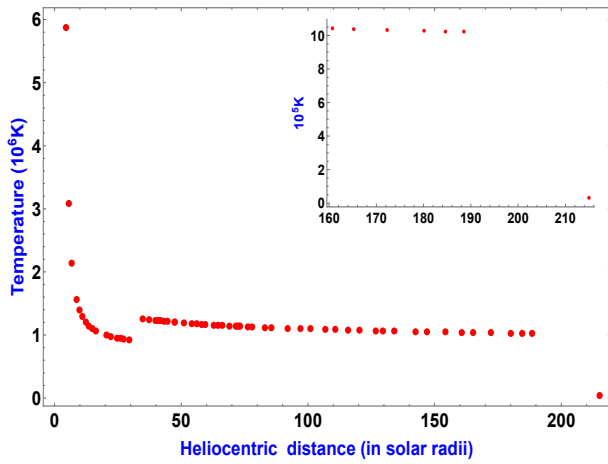
Our first data point is around 4 solar radii. Generally the temperature of the first data point is in between the orders 10^5 to 10^6 K. Lee et al. (2009) [15] have estimated the temperature of a blob of plasma of a CME at a distance of 4 solar radii to be about 10^6 K by employing various models of plasma heating. Akmal et al. (2001) [1] have done a similar estimation of 10^5 K. Our results match their estimation. If we compare the temperature at the last data point and the 1 AU value, we can observe that there is a temperature drop of orders of 10^5 K.



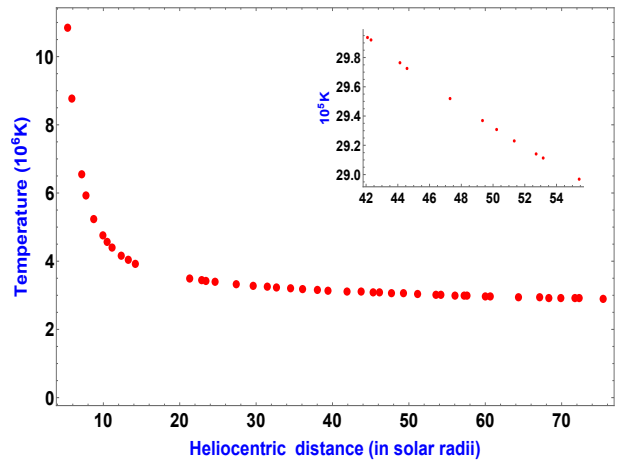
CME 1



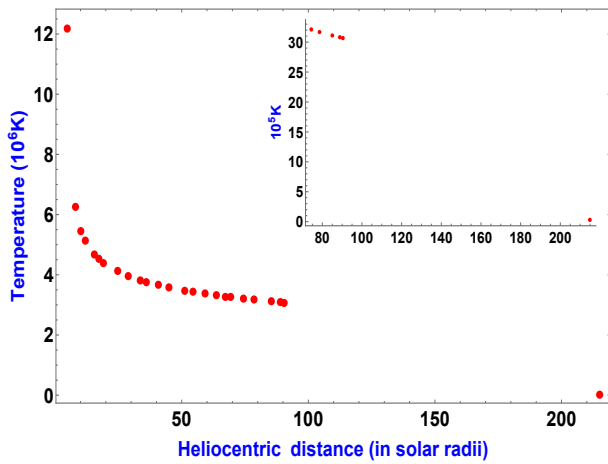
CME 5



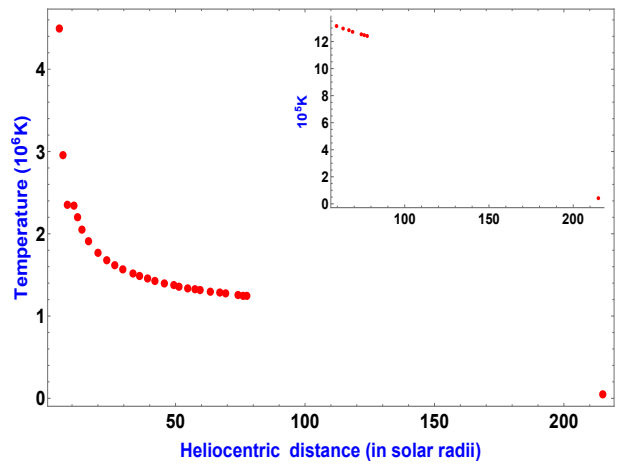
CME 9



CME 20

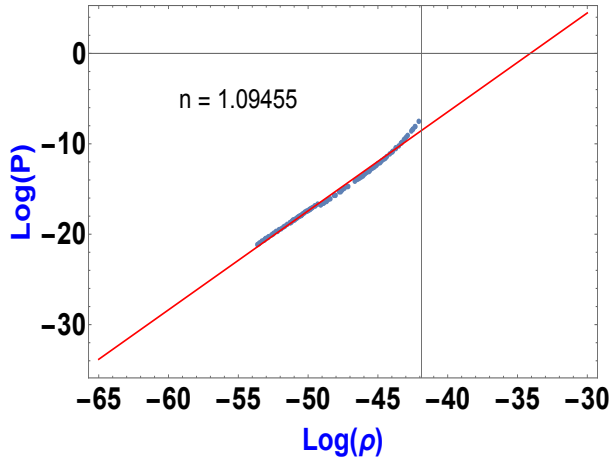


CME 33

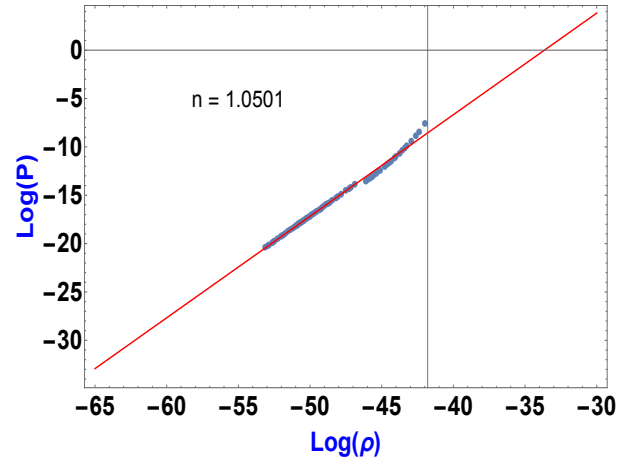


CME 36

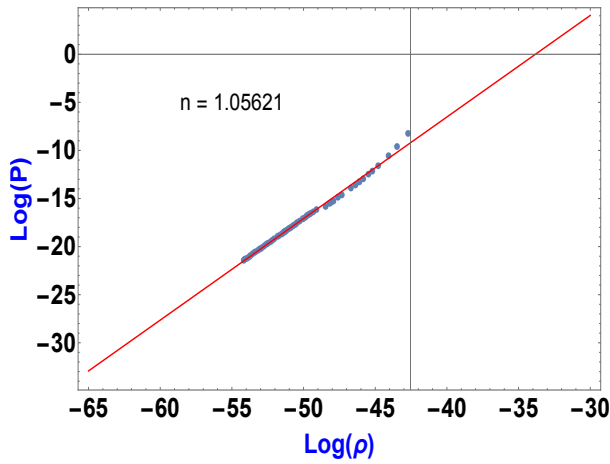
6.2 Polytropic Index



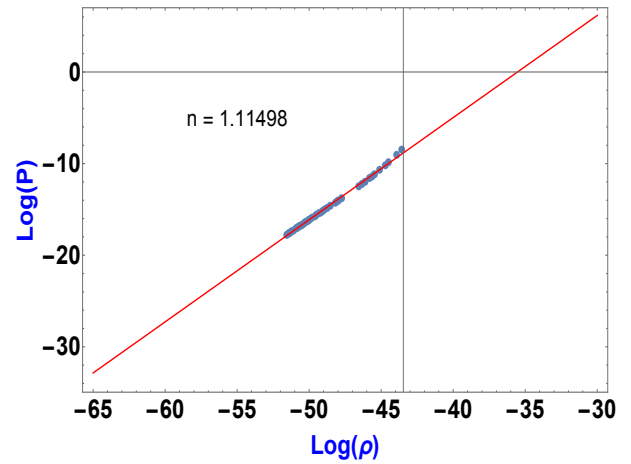
CME 1



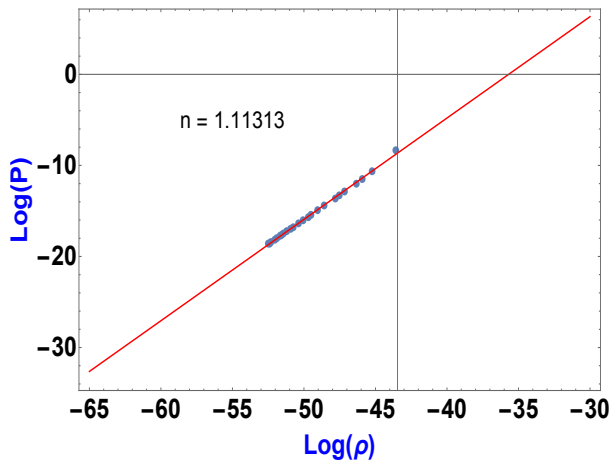
CME 5



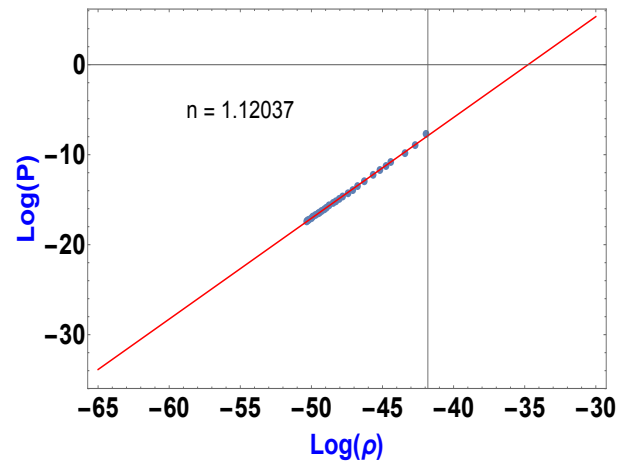
CME 9



CME 20



CME 33



CME 36

The above are examples of the linear fits of Log(pressure) vs Log(density). As we can see that the data points match the linear fit well. I plotted a histogram for polytropic index of all the CMEs.

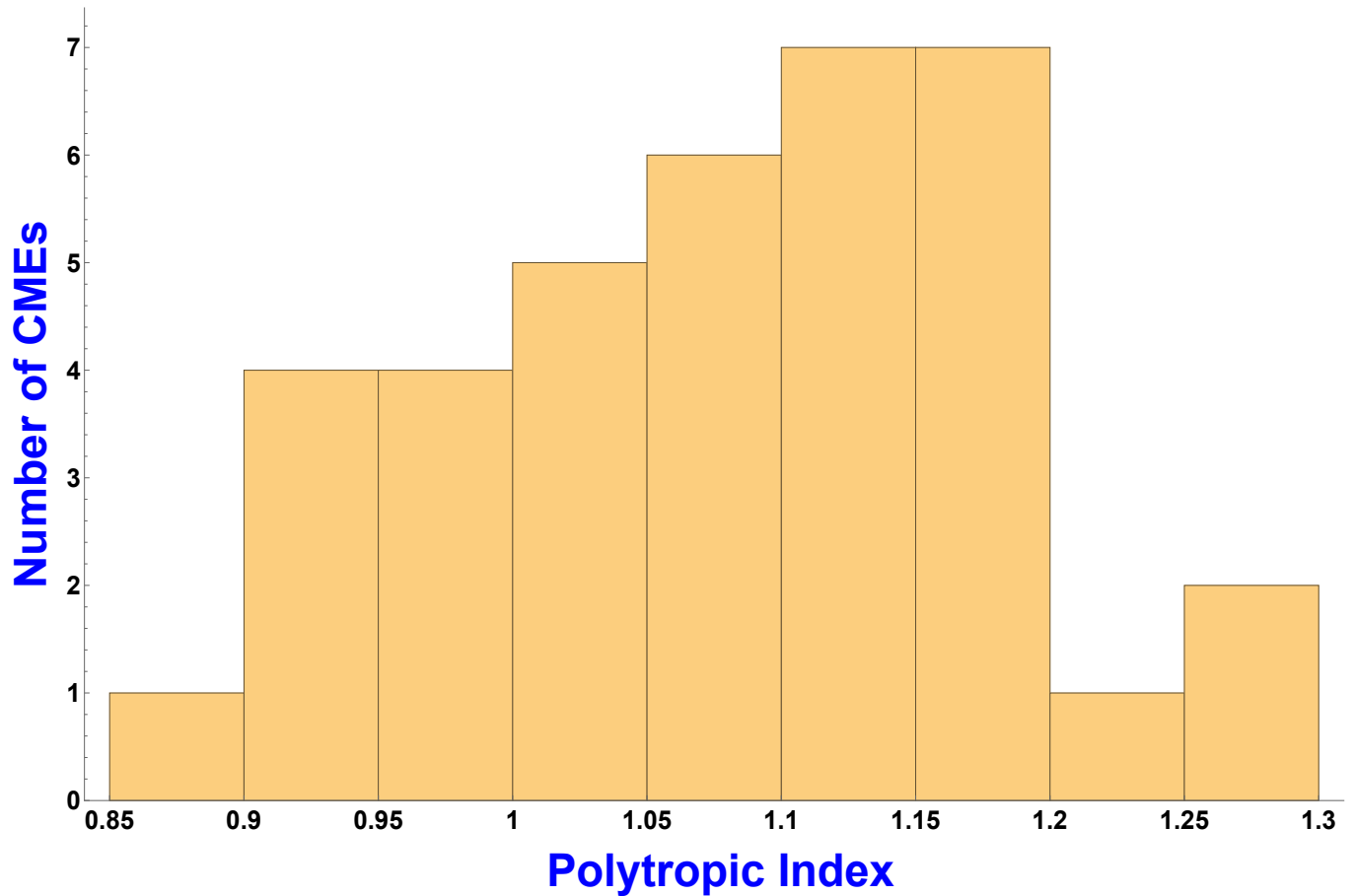
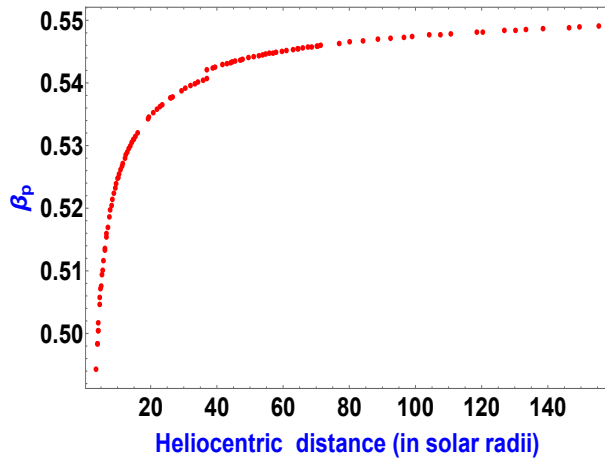


Figure 6.13: Histogram of polytropic index

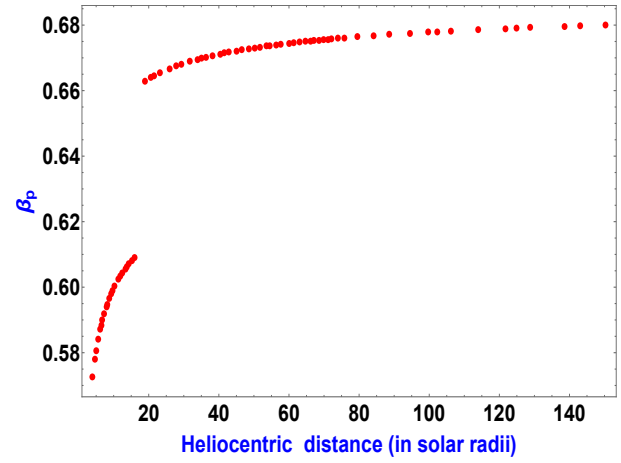
Most of the CMEs have polytropic index greater than 1. This result confirms that there is heating in CME plasma which we wanted to study in my thesis. The value of polytropic index quantifies plasma heating. However, there are a few CMEs whose polytropic index is less than 1 but very near to 1. This could be due to the sensitivity in fitting of data.

6.3 β_p and Plasma Beta Profiles

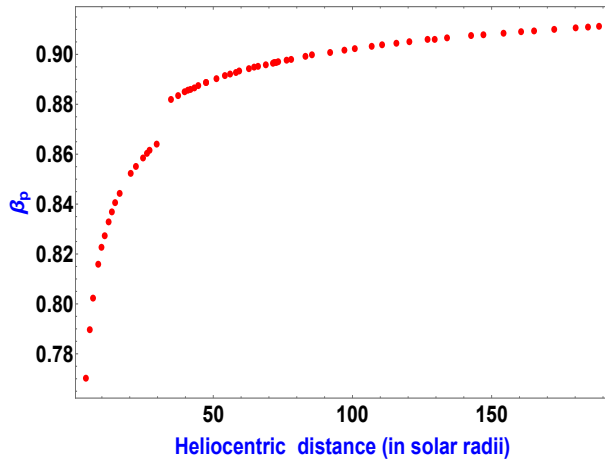
We can observe that generally, plasma beta increases as CMEs expand. We have proved and quantified our assumption that contribution of thermal pressure increases as the CME expands.



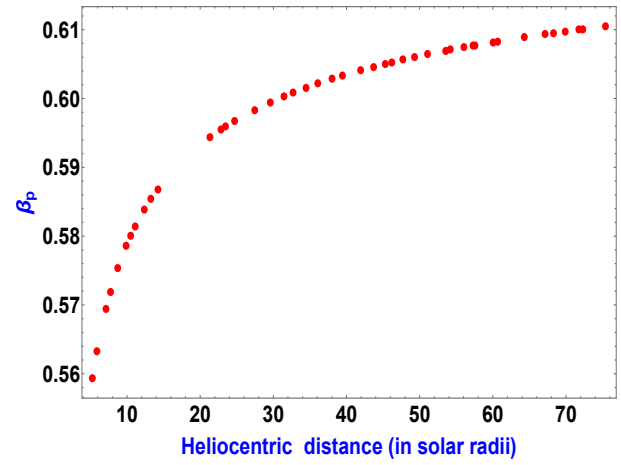
CME 1



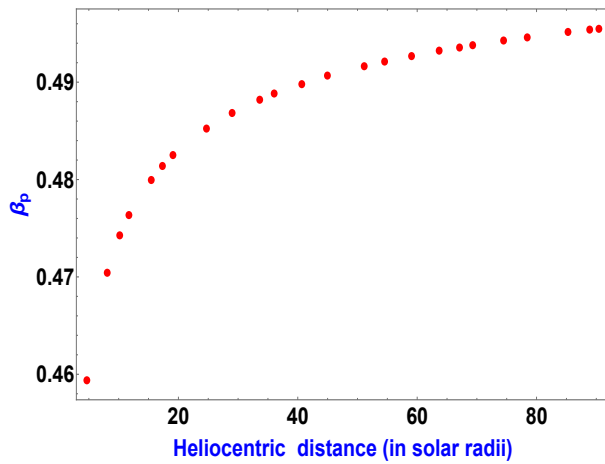
CME 5



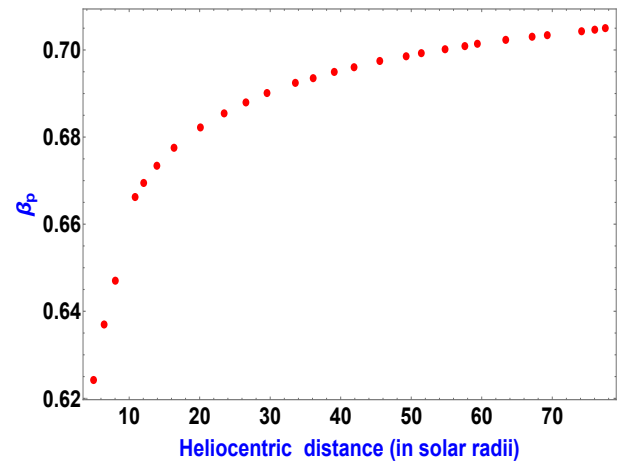
CME 9



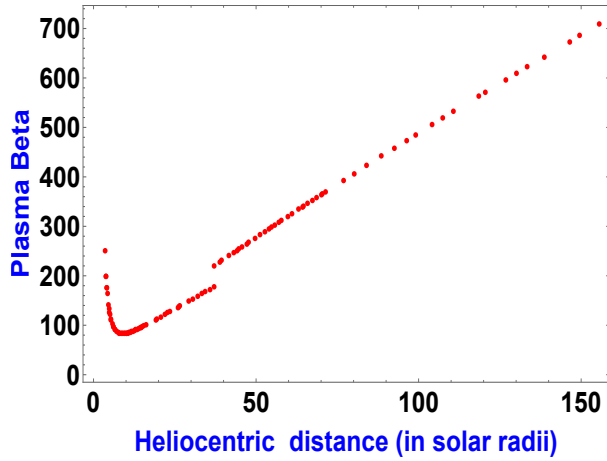
CME 20



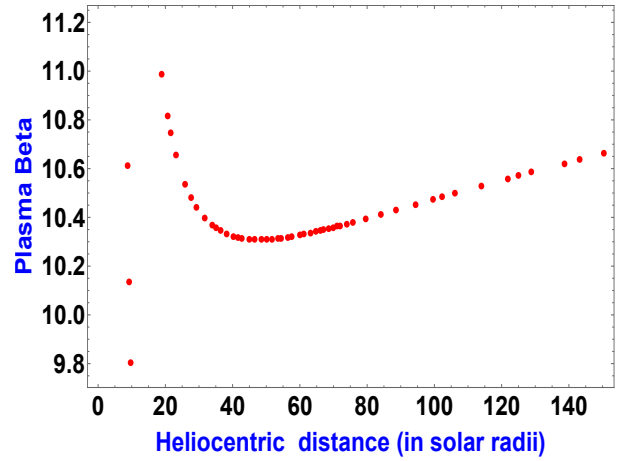
CME 33



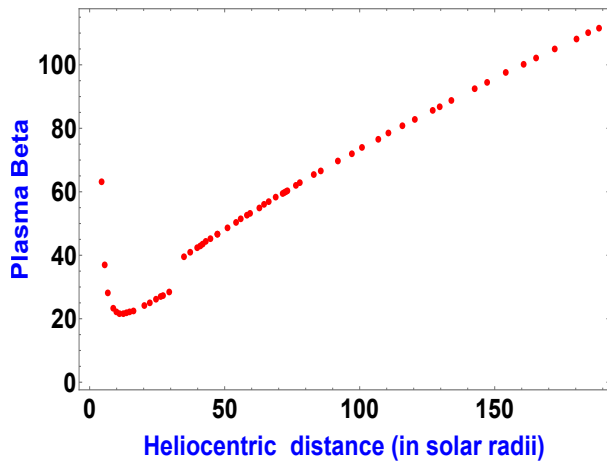
CME 36



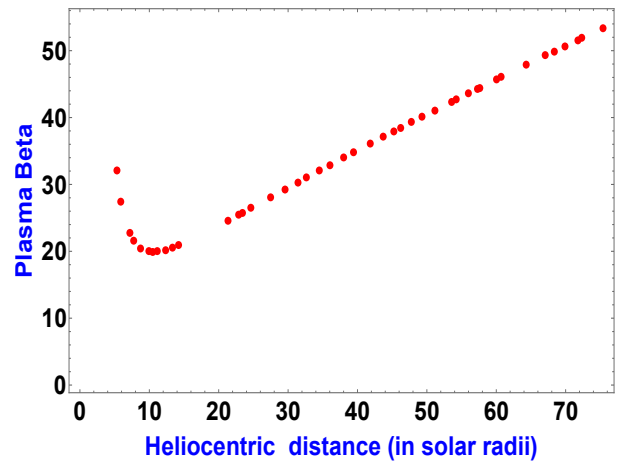
CME 1



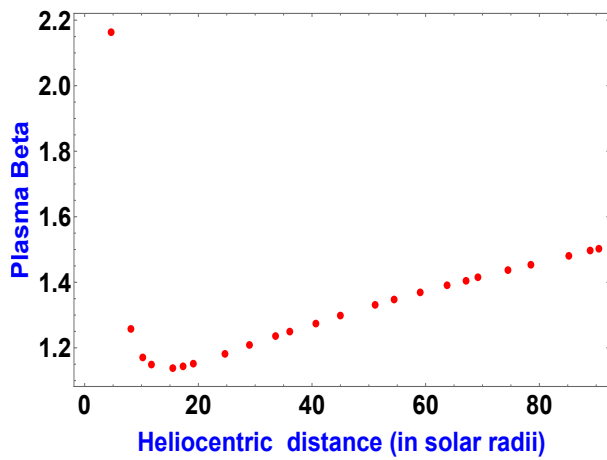
CME 5



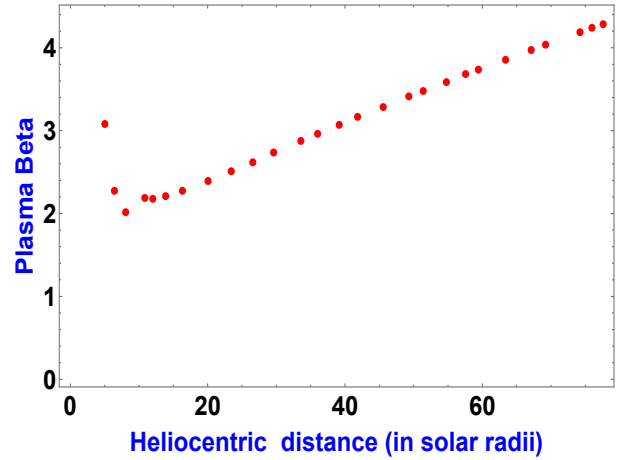
CME 9



CME 20

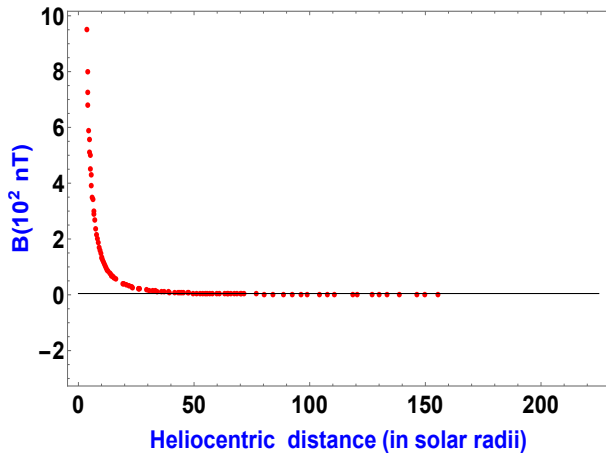


CME 33

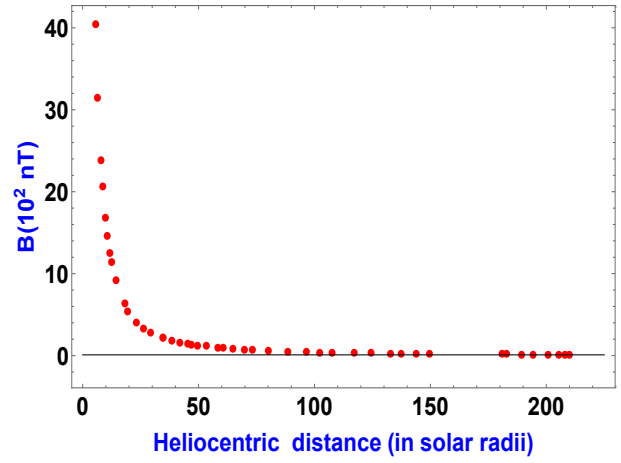


CME 36

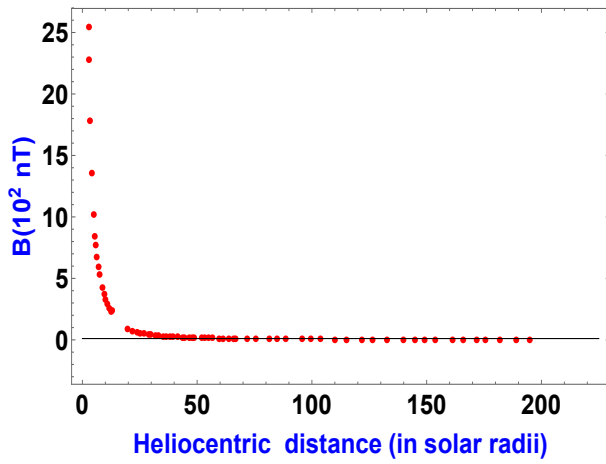
6.4 Magnetic Field Profiles



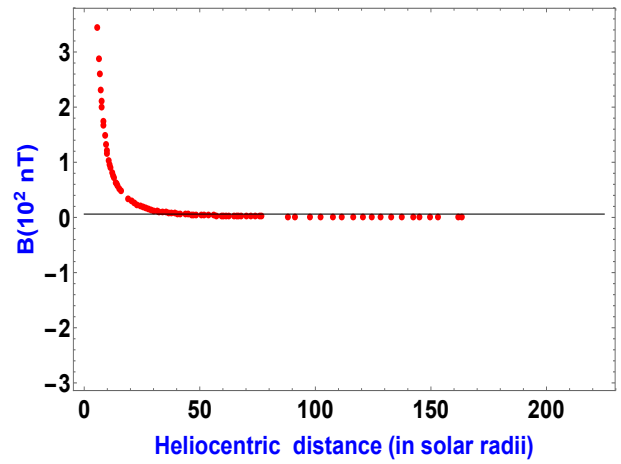
CME 1



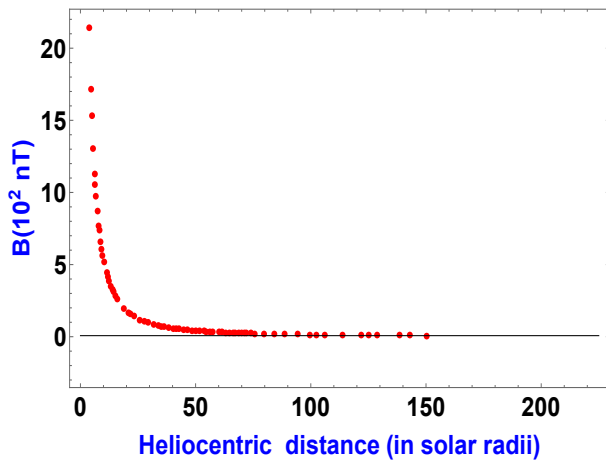
CME 2



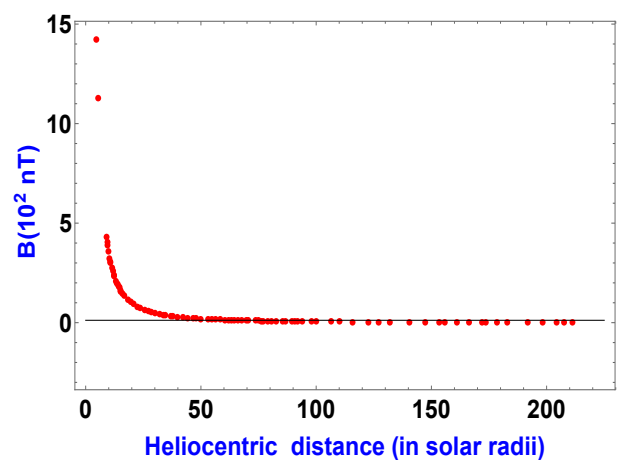
CME 3



CME 4



CME 5



CME 11

In the above plots, The black line is the observed value of magnetic field at 1 AU. We can observe that the profile tends to match very well with black line at 1AU. I extrapolated the values of the estimated magnetic field profile and estimated the error in these extrapolated values wrt. to the observed values at 1 AU and plotted the following histogram

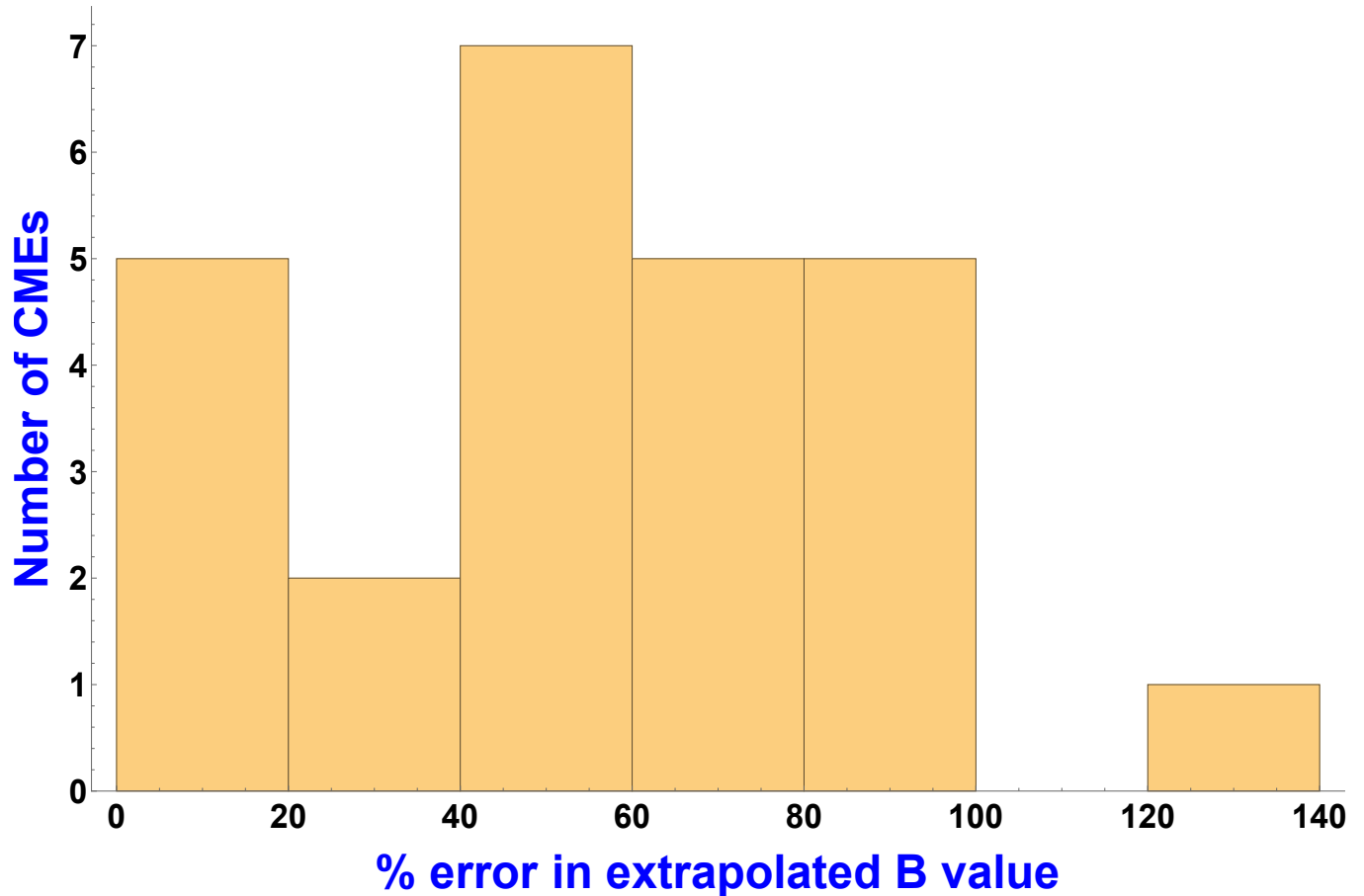
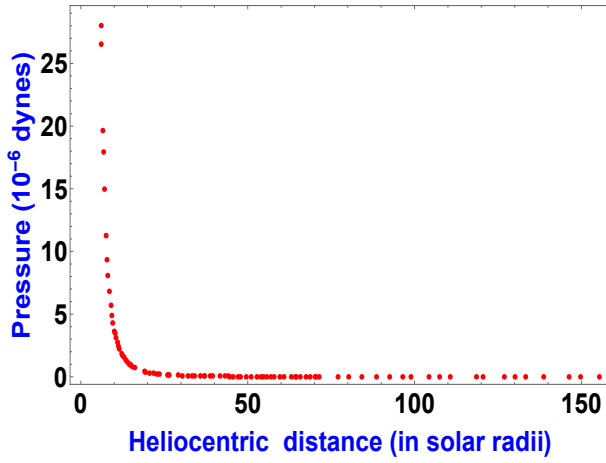


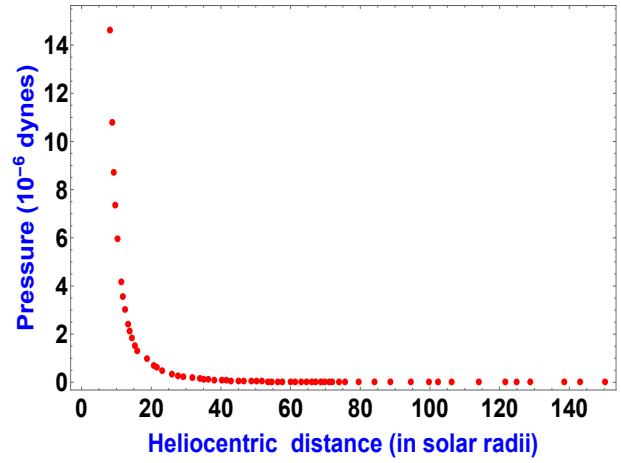
Figure 6.32: Error in extrapolated B values

Most of the CMEs have an error less than 100 %. This is very good considering that each unit on y axis measures 100 nT and the observed values are of the order of 10 nT. Even a slight variation in extrapolation would give values off hundreds of nTs. The profile of magnetic field is estimated using I_t values from the GCS model and force free solutions. Hence, we can conclude that the data from the GCS fitting is good and force-free approximation is reasonable.

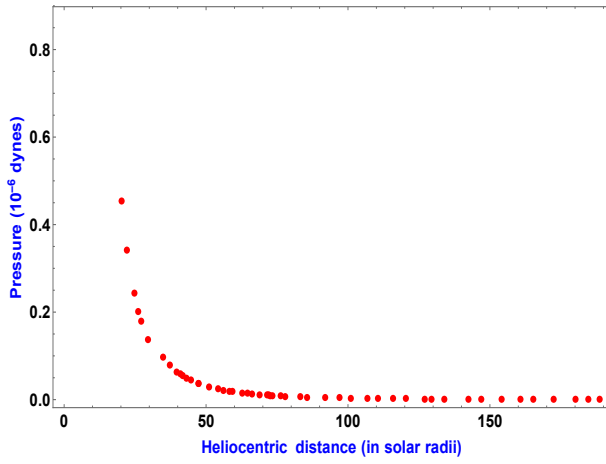
6.5 Pressure Profiles



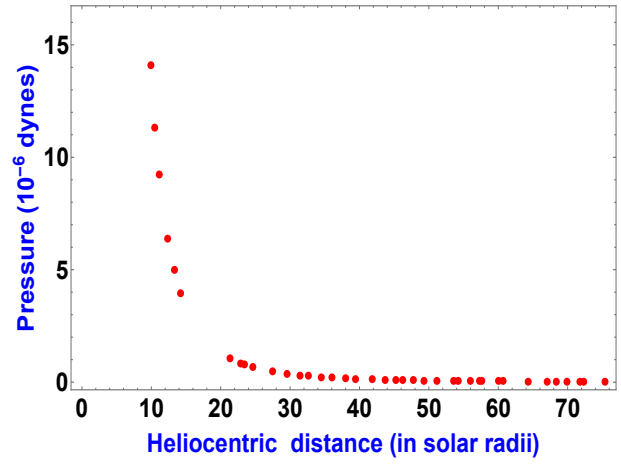
CME 1



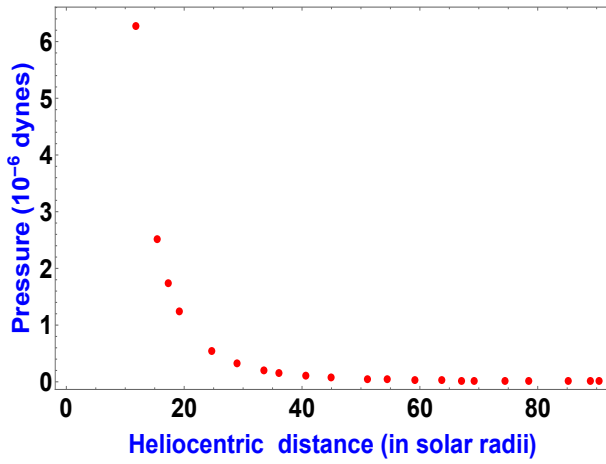
CME 5



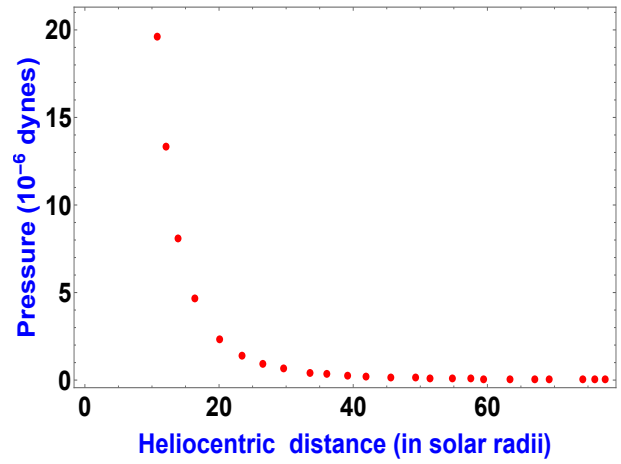
CME 9



CME 20

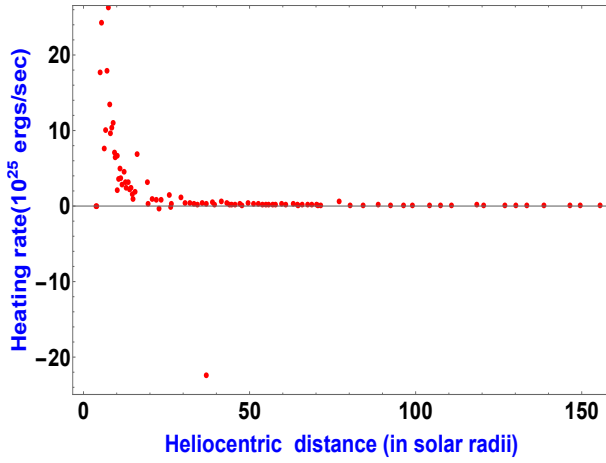


CME 33

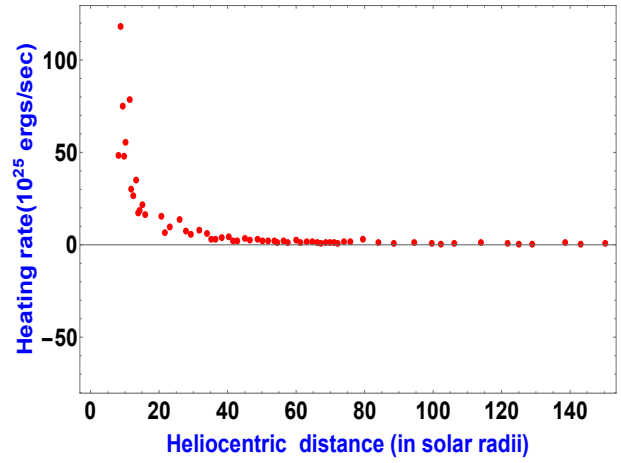


CME 36

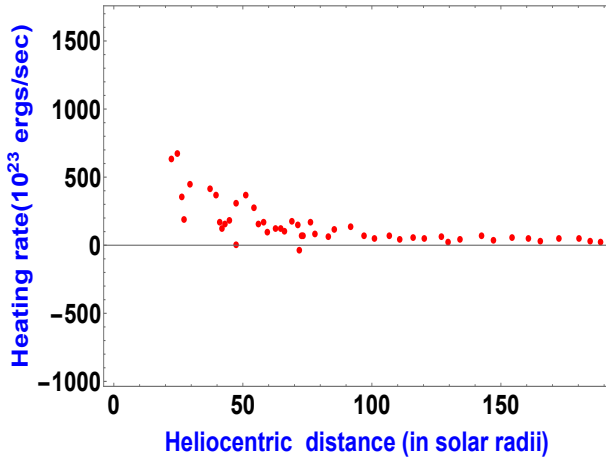
6.6 Heating Budget and Rates



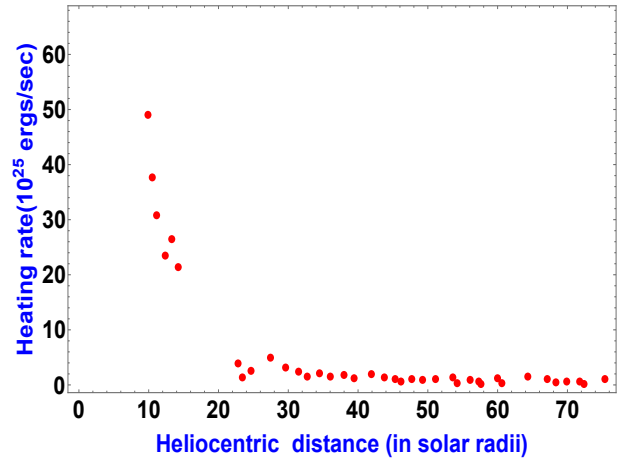
CME 1



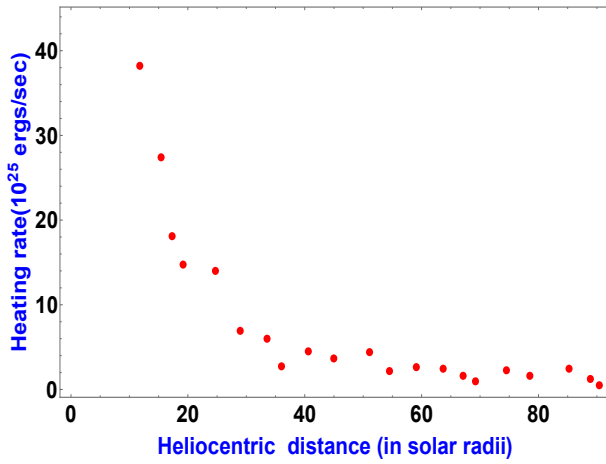
CME 5



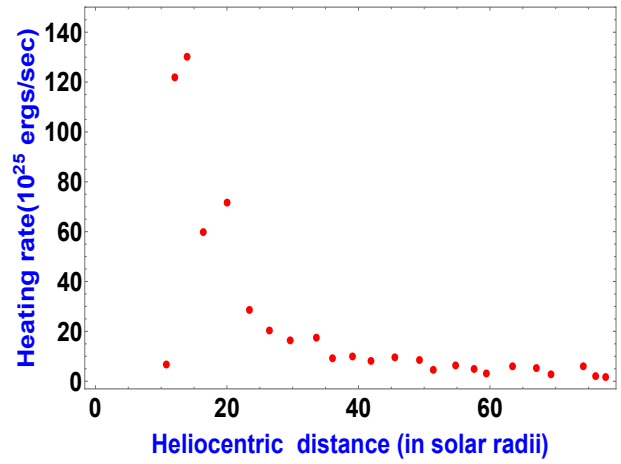
CME 9



CME 20



CME 33



CME 36

The above figures are the plots of average heating rates between consecutive data points with heliocentric distance. Generally, the average heating rates are of the order of 10^{26} ergs/s at heliocentric distances of 4 - 6 solar radii. The time period between which these rates are of the order 10^3 seconds. So the heating budgets at 4 - 6 solar radii heliocentric distance is of the order 10^{29} ergs. Mass of a CME in our sample is around 10^{15} grams. So the heating budget estimate would be of the order 10^{14} ergs/gram. Lee et al. (2009) [15] have studied atomic emission lines of several blobs of plasma at a distance of about 2-6 solar radii of a CME that occurred on Dec 13th 2001. They estimated number density and further heating energy of these blobs to be of the order of 10^{14} to 10^{15} ergs/gram which agrees with our results. Akmal et al. (2001) [1] have also done a similar estimation for a CME which occurred on April 23, 1999 and have estimated the heating energy to about 10^{15} ergs/gram up to 3.5 solar radii distance. Murphy et al. (20011) [19] have done a similar estimate of about 10^{14} ergs/gram for a CME which occurred on June 28, 2000.

$$\text{Number of protons in a CME} = \frac{\text{Mass of the CME}}{\text{proton mass}} = \frac{10^{15}}{1.67 \times 10^{-24}} \approx 10^{39}$$

Number of protons of a CME in our sample would be of the order of 10^{39} . Then the heating budget is of the order of 10^{-10} ergs/proton. Ciaravella et al. (2001) [8] have estimated using atomic spectra the heating budget to be of the order of 10^{-10} ergs/proton at a distance of 1.7 solar radii, which agrees with our results.

At the first point of data at about 5 solar radii the volume of a CME is about 10^{33}cm^3 for a semi-torus assumed in our analysis. Then the heating rates would be of the order of 10^{-7} ergs $s^{-1} \text{cm}^{-3}$. Lee et al. (2009) [15] have estimated a heating rate of 5×10^{-7} ergs $s^{-1} \text{cm}^{-3}$ which is in good agreement with our results. It tells us that our estimate of volume is also reasonable. In the distance between 9 to 20 solar radii, the volume of CMEs is of the order 10^{35}cm^3 and the heating rates in this distance range would be around 10^{-9} ergs $s^{-1} \text{cm}^{-3}$ according to us. Sasikumar Raja et al. (2017) [22] have estimated the heating rates in solar wind in this distance range to be between 10^{-11} and 10^{-13} ergs $s^{-1} \text{cm}^{-3}$. So, we can conclude that the heating rate in CME is much higher than in the solar wind.

Chapter 7

Conclusions

We had speculated that while Lorentz force drives the expansion of CME length, it would lead to contraction of the cross-section. But the cross-section of CMEs is observed to expand. So, we predicted that the effect of gas pressure increases in CME dynamics as it evolves. Also, the near earth temperatures indicated that the expansion of CMEs is far from being adiabatic and we supposed that there is heating of plasma. We sought to understand the thermodynamics of CME evolution in a better manner. We analyzed data obtained by fitting the GCS model to a set of well observed, Earth-directed CMEs. We also assumed force-free approximation for the structure of magnetic field lines within the CMEs.

We have estimated profiles of physical quantities which are temperature, pressure and plasma beta. This would serve to study the energetics of these CMEs. We have scrutinize the effect of Lorentz force on the dynamics of a CME by decomposing it into magnetic tension and pressure forces. We have rigorously demonstrated that Lorentz forces indeed are responsible for contraction of the cross-section of CMEs. I have also attempted to reconstruct the force equations along major and minor radii of a CME torus by demonstrating the action of magnetic pressure and tension forces as well as gas pressure.

The plasma beta generally increases as the CME evolves confirming our supposition that the contribution of pressure increases as the CME evolves. We have estimated polytropic index for the evolution of each CME. The value of the polytropic index represents the extent of heating

or cooling occurring in a CME as it evolves. The value of the polytropic index for most of the CMEs is greater than 1. This result confirms that there is indeed plasma heating in CMEs. Using temperature profile and polytropic index, we have a crude estimate of heating budget and heating rate profile of each CME. These estimates are in good agreement with many other estimates in the literature. This result can be further used to study the possible dissipation of magnetic energy through turbulence to heat the plasma.

We have estimated the profile of the magnetic field as the CME evolves using data from GCS fitting and assuming Force-free configuration for the magnetic field. We have extrapolated this profile to 1 AU and compared it with the observed value from WIND spacecraft. The extrapolated values agree very well with the observed values. This indicates that our data obtained from GCS fitting (by Sachdeva et al.) is plausible and also that Force-free approximation for magnetic fields of CMEs is a reasonable approximation.

Chapter 8

Appendix

8.1 Another Method to Estimate β_p and Temperature Profiles

In this method we sought to estimate the same quantities through a different method. Writing the major and minor radial equations again.

$$\frac{M\ddot{R}}{2\pi R} = \frac{I_t^2}{c^2 R} \left[\ln\left(\frac{8R}{a}\right) + \frac{\beta_p}{2} - \frac{1}{2} \frac{\overline{B}_t^2}{B_{pa}^2} - 2\left(\frac{R}{a}\right) \frac{B_s}{B_{pa}} - 1 + \frac{\xi_i}{2} \right]$$

$$\frac{M\ddot{a}}{2\pi R} = \frac{I_t^2}{c^2 a} \left[\frac{\overline{B}_t^2}{B_{pa}^2} - 1 + \beta_p \right]$$

We multiply the first equation and add it to the next equation, and substitute $\xi = 1$,

$$\frac{MR\ddot{R}}{\pi R} + \frac{Ma\ddot{a}}{2\pi R} = \frac{I_t^2}{c^2} \left[2\ln\left(\frac{8R}{a}\right) + \beta_p - \frac{\overline{B}_t^2}{B_{pa}^2} - 4\left(\frac{R}{a}\right) \frac{B_s}{B_{pa}} - 1 - 1 + \frac{\overline{B}_t^2}{B_{pa}^2} + \beta_p \right]$$

$$\frac{c^2 M}{2\pi I_t^2 R} \left(R\ddot{R} + \frac{a\ddot{a}}{2} \right) = \ln\left(\frac{8R}{a}\right) + \beta_p - 2\left(\frac{R}{a}\right) \frac{B_s}{B_{pa}} - 1$$

$$\beta_p = \frac{c^2 M}{2\pi I_t^2 R} \left(R\ddot{R} + \frac{a\ddot{a}}{2} \right) - \ln\left(\frac{8R}{a}\right) + 2\left(\frac{R}{a}\right) \frac{B_s}{B_{pa}} + 1 \quad (8.1)$$

$$\frac{8\pi(p - p_a)}{B_{pa}^2} = \frac{c^2 M}{2\pi I_t^2 R} \left(R\ddot{R} + \frac{a\ddot{a}}{2} \right) - \ln\left(\frac{8R}{a}\right) + 2\left(\frac{R}{a}\right) \frac{B_s}{B_{pa}} + 1$$

Again substituting for B_{pa} , $B_{pa} = \frac{2I_t}{ca}$

$$\frac{2\pi c^2 a^2 (p - p_a)}{I_t^2} = \frac{c^2 M}{2\pi I_t^2 R} \left(R\ddot{R} + \frac{a\ddot{a}}{2} \right) - \ln\left(\frac{8R}{a}\right) + 2\left(\frac{R}{a}\right) \frac{B_s}{B_{pa}} + 1$$

$$p = \frac{M}{4\pi^2 a^2 R} \left(R\ddot{R} + \frac{a\ddot{a}}{2} \right) + \left(1 - \ln\left(\frac{8R}{a}\right) \right) \frac{I_t^2}{2\pi c^2 a^2} + \left(\frac{I_t R B_s}{2\pi c a^2} \right) + p_a \quad (8.2)$$

Again using, $p = 2nk_b T \implies T = \frac{p}{2nk_b}$

$$T = \frac{\pi^2 a^2 R m_p}{2k_b M} \left[\frac{M}{4\pi^2 a^2 R} \left(R\ddot{R} + \frac{a\ddot{a}}{2} \right) + \left(1 - \ln\left(\frac{8R}{a}\right) \right) \frac{I_t^2}{2\pi c^2 a^2} + \frac{I_t R B_s}{2\pi c a^2} + p_a \right] \quad (8.3)$$

In this method, we need to find the values of \ddot{R} and \ddot{a} . We had the profiles of R and a as a function of time. We had to fit these profiles and then take the double derivative of the fit to get \ddot{R} and \ddot{a} . But there were several possible fits and each fit gave a different acceleration profile and hence temperature profiles. We had no solid ground to decide which fit gave the best estimates of the temperature profile.

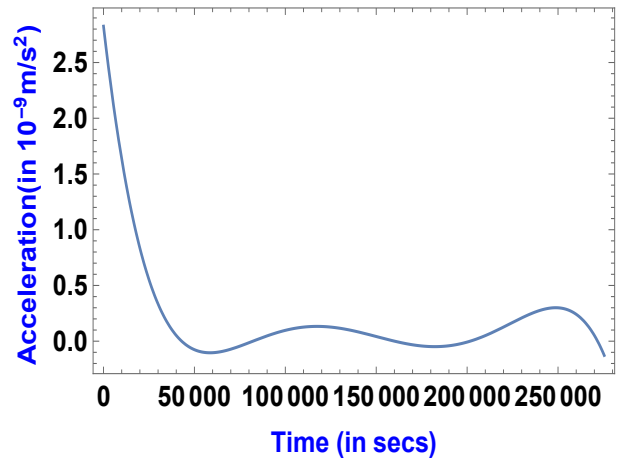
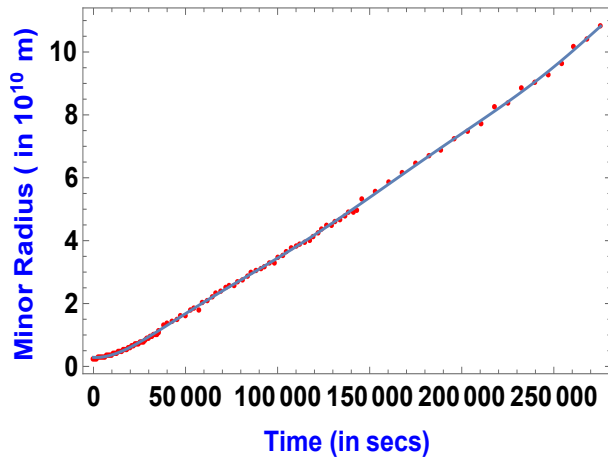


Figure 8.1: 7th order polynomial fit

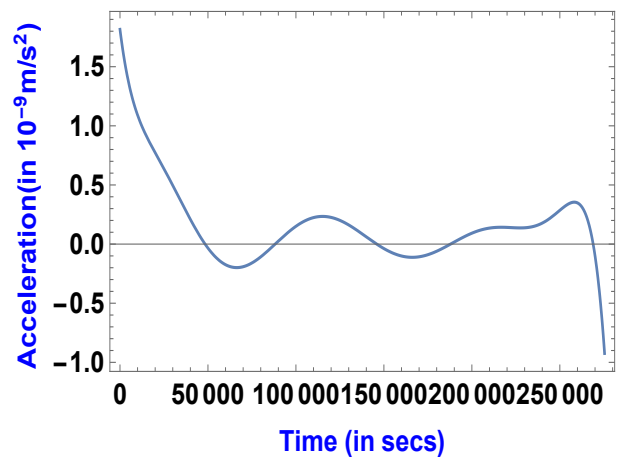
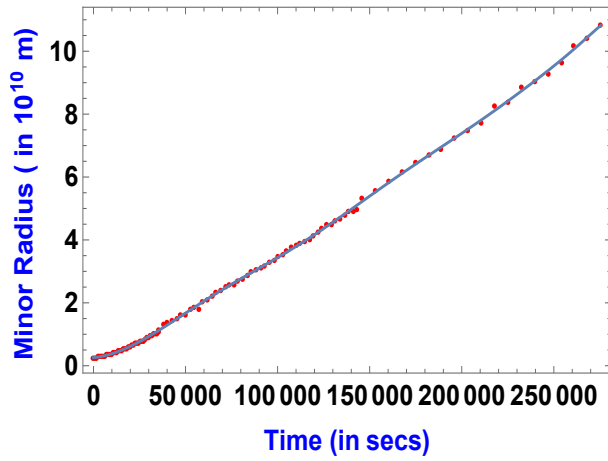


Figure 8.2: 11th order polynomial fit

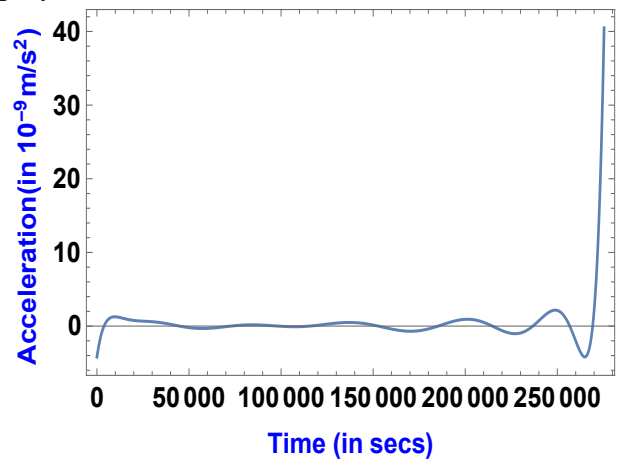
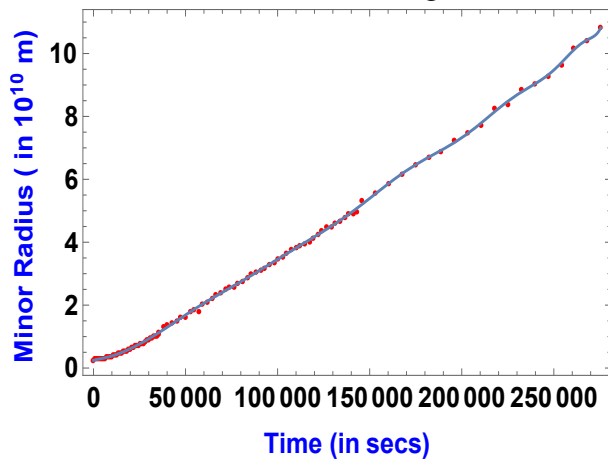


Figure 8.3: 15th order polynomial fit

8.2 Correction to Force-free Solutions

In the force free solutions 4.2, we have assumed cylindrical symmetry, neglecting the effects of curvature of the torus. As R is the major radius of the curvature, $\frac{1}{R}$ gives the curvature of the torus. κ being proportional to $\frac{1}{R}$, quantifies curvature of the torus. Berdichevsky (2013) [3] suggested correction to the force free solution in the argument of the Bessel's functions.

$$A(y, \phi) = x_0 y [1 + \kappa y (\cos \phi - |\sin \phi|)] \quad (8.4)$$

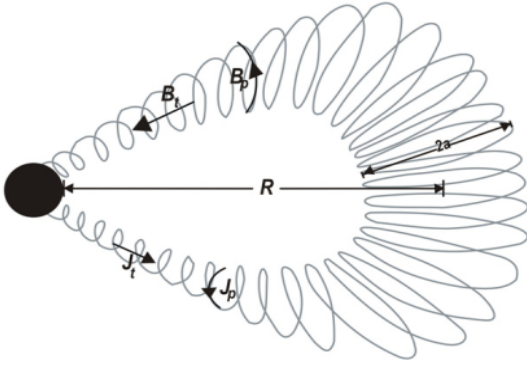


Figure 8.4: Curvature of helical fields due to curvature of CME torus

Credits: Subramanian et al. (2014) [25]

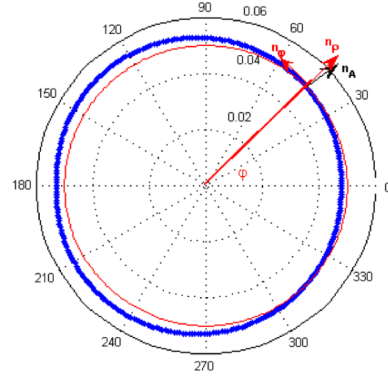


Figure 8.5: Non-overlapping of adjacent rings of magnetic field due to curvature of CME torus

Credits: Berdichevsky (2012) [3]

The above correction accounts for the non-overlapping of two consecutive rings of magnetic field lines in a flux rope. If the flux rope were exactly cylindrical, all the rings would exactly overlap, but due to the toroidal shape, two adjacent rings cut only at two points.

We tried to account this correction while calculating $\frac{\overline{B_t^2}}{B_{pa}^2}$. We took average value, by taking average over ϕ ,

$$\frac{\overline{B_t^2}}{B_{pa}^2} = 4 \left[\frac{\int_0^1 \int_0^{2\pi} J_0(x_0[y + \kappa y^2(\cos \phi - |\sin \phi|)]) y d\phi dy}{\int_0^{2\pi} J_1(x_0[1 + \kappa(\cos \phi - |\sin \phi|)]) d\phi} \right]^2 \quad (8.5)$$

We got negative β_p values using the corrected values for $\frac{\overline{B_t^2}}{B_{pa}^2}$

8.3 Mathematica Codes

8.3.1 Physical quantities profiles of CME

```
A = Import["F:\\Project\\Input\\1.xlsx"];
(*Importing data from an excel file named "1.xlsx" from the location "F:\\Project\\Input\\"
which has time, apex distance, minor radius, kappa, It, external magnetic field of CME 1 in the 1st,
2nd, 3rd, 4th, 6th and 7th column repectively*)

t = A[[1, All, 1]];
Z = A[[1, All, 2]];
a = A[[1, All, 3]];
K = A[[1, All, 4]];
It = A[[1, All, 6]];
Bs = A[[1, All, 7]];
k = Mean[K]; (* calculating average kappa *)
H = Z - a; (* calculating major radius *)
kb = 1.38064852 × 10-16; (* Boltzmann's constant in cgs *)
M = 2.9 × 1015; (* Mass of CME 1 from Nishtha's thesis in grams *)
V = π2 * a2 * H * (6.957 × 1010)3; (* calculating volume of CME assuming it is a semi-torus *)
ρ = M / V; (* calculating average density of CME 1 *)

na = (3.6 / 7.2) * ((8 × 107 * H-6) + (4.1 × 106 * H-4) + (3.3 × 105 * H-2));
(* number density of ambient solar wind as a function of heliocentric distance *)
Ta = 1.654 * ((197 * 22) + 57 300) * (H / 215)-1.1;
(* temperature of ambient solar wind as a function of heliocentric distance *)
pa = 2 * na * kb * Ta; (* pressure of ambient solar wind as a function of heliocentric distance *)
L = Length[a]

f[i_] := (2 * k2 / (2 - k2) * (Log[8/k] - (0.691556 * (2 + k2) / (2 * k2))) - (Bs[[i]] * H[[i]] * 6.957 × 1011) / It[[i]]) + 1;
β = Table[f[i], {i, 1, L}] // FullSimplify; (* evaluating βp profile *)
e[i_] := (0.04 * It[[i]]2 / (8 π * (a[[i]] * 6.957 × 1010)2) * (β[[i]])) + pa[[i]];
p = Table[e[i], {i, 1, L}] // FullSimplify; (* evaluating pressure (in cgs units) profile *)

m = 1.6726219 × 10-24;
(* mass of proton in grams *)
```



```

g[i_] :=  $\frac{p[[i]] * m}{2 * k_b * \rho[[i]]}$ ;
T2 = Table[g[i], {i, 1, L}] // FullSimplify; (* evaluating temperature profile *)

j[i_] :=  $\beta[[i]] + \frac{p_a[[i]] * 200 * \pi * (a[[i]] * 6.957 \times 10^{10})^2}{(I_t[[i]])^2}$ ;
 $\beta_1$  = Table[j[i], {i, 1, L}] // FullSimplify; (* evaluating plasma beta profile *)

BP1 = Thread[{Z,  $\beta_1$ ]];
ListPlot[BP1, Frame → {True, True, True, True},
  FrameLabel → {Text@Style["Heliocentric distance (in solar radii)", Bold, {Blue}],
    Text@Style["Plasma Beta", Bold, {Blue}]}, LabelStyle → {FontSize → 30, Bold, {Black}},
  PlotStyle → {Red, Thick}] (* Plotting plasma beta profile *)

ListPlot[Thread[{Z,  $p * 10^6$ }], Frame → {True, True, True, True},
  FrameLabel → {Text@Style["Heliocentric distance (in solar radii)", Bold, {Blue}],
    Text@Style["Pressure ( $10^{-6}$  dynes)", Bold, {Blue}]}, LabelStyle → {FontSize → 30, Bold, {Black}},
  PlotStyle → {Red, Thick}] (* Plotting pressure profile *)

BP = Thread[{Z,  $\beta$ ]];
ListPlot[BP, Frame → {True, True, True, True},
  FrameLabel → {Text@Style["Heliocentric distance (in solar radii)", Bold, {Blue}],
    Text@Style[" $\beta_p$ ", Bold, {Blue}]}, LabelStyle → {FontSize → 30, Bold, {Black}},
  PlotStyle → {Red, Thick}, PlotRange → All] (* Plotting  $\beta_p$  profile *)

lnP = Log[p];
ln $\rho$  = Log[ $\rho$ ];
P = Thread[{ln $\rho$ , lnP}];
f1 = FindFit[P, c y + b, {c, b}, y] (* fitting log(p) vs log( $\rho$ ) with a linear fit *)
n = c /. f1 (* value of polytropic index *)

f2 = Fit[P, {1, y}, y]

f4 = Plot[f2, {y, -65, -30}, PlotStyle → {Red, Thick}, Frame → {True, True, True, True},
  FrameLabel → {Text@Style["Log( $\rho$ )", Bold, {Blue}], Text@Style["Log(P)", Bold, {Blue}]},
  LabelStyle → {FontSize → 34, Bold, {Black}}];

f3 = ListPlot[P, Frame → {True, True, True, True},
  FrameLabel → {Text@Style["Log( $\rho$ )", Bold, {Blue}], Text@Style["Log(P)", Bold, {Blue}]},
  PlotStyle → {Thick}, Epilog → Style[Text[StringForm["n = `", n], {-55, -5}], 30]];
Show[f3, f4, PlotRange → All, LabelStyle → {FontSize → 35, Bold, {Black}}]
(* Plotting log(p) vs log( $\rho$ ) along with the fit and polytropic index *)

```

```

h = Append[Z, 215];
T = Append[T2, 8362.13]; (* appending 1 AU data from WIND data *)
Temp = Thread[{h, T/106}]];
N1 = Drop[h, 99];
N2 = Drop[T, 99];

d = ListPlot[Thread[{N1, N2/105}], PlotRange → All, Frame → {True, True, False, False},
  FrameLabel → {None, Text@Style["105K", Bold, Blue]}, LabelStyle → {FontSize → 25, Bold, {Black}},
  PlotStyle → {Red, Thick}]; (* creating an inset d,
which is the temperature profile of near earth heliocentric distances *)

ListPlot[Temp, Frame → {True, True, True, True},
  FrameLabel → {Text@Style["Heliocentric distance (in solar radii)", Bold, {Blue}],
  Text@Style["Temperature (106K)", Bold, {Blue}]}], LabelStyle → {FontSize → 30, Bold, {Black}},
  PlotStyle → {Red, Thick},
  Epilog → Inset[d, Scaled[{.5, .5}], Scaled[{0, 0}], 120], PlotRange → All, PlotRangeClipping → False]
(* Plotting temperature profile of CME 1 *)
f[i_] := 
$$\frac{83144621 * M * (T2[[i]] - T2[[i + 1]]) * (1.66667 - n)}{0.66667 * (n - 1)}$$
;
Q = Table[f[i], {i, 1, L - 1}] // FullSimplify
(* evaluating heating budget between adjacent data points *)

j[i_] := 
$$\frac{Q[[i]]}{t[[i + 1]] - t[[i]]}$$
;
G = Table[j[i], {i, 1, L - 1}] // FullSimplify
(* evaluating average heating rate between adjacent data points *)

H1 = Drop[Z, 1];
ListPlot[Thread[{H1, G/1025}], Frame → {True, True, True, True},
  FrameLabel → {Text@Style["Heliocentric distance (in solar radii)", Bold, {Blue}],
  Text@Style["Heating rate (1025 ergs/sec)", Bold, {Blue}]}],
  LabelStyle → {FontSize → 30, Bold, {Black}}, PlotStyle → {Red, Thick}]
(* plotting heating rate profile *)

```

8.3.2 Magnetic field profile and extrapolation at 1 AU

```
A = Import["F:\\Project\\MF\\Excel\\magnetic_field_event_1.csv"];
(*Importing data from an excel file which has heliocentric distance of CME apex in the
 1st and 2nd columns repectively*)
A1 = A[[All, 1]]; A3 = Drop[A1, 1];
A2 = A[[All, 2]]; A4 = Drop[A2, 1];
L = Length[A3];
H = Delete[A3, L]; B = Delete[A4, L];
b = A4[[L]]; (* observed 1 AU value *)
a = b/100;
f1 = ListPlot[Thread[{H, B/100}], PlotStyle -> {Red, Thick}];
f2 = Graphics@Line[{0, a}, {225, a}];

Show[f1, f2, AxesOrigin -> {0, -3}, PlotRange -> All, Frame -> {True, True, True, True},
  FrameLabel -> {Text@Style["Heliocentric distance (in solar radii)", Bold, {Blue}],
    Text@Style["B(102 nT)", Bold, {Blue}]}, LabelStyle -> {FontSize -> 25, Bold, {Black}}]
(* plotting B profile along with 1 AU value *)

(* 1. Extrapolation of B value at 1 AU by interpolating *)
H1 = Drop[H, 67]; B1 = Drop[B, 67];
K1 = Thread[{H1, B1}]; (* B profile is shortened by removing initial part where B
falls drastically *)
Y = Interpolation[K1, Method -> "Spline", InterpolationOrder -> 3];
Y3 = Plot[Y[z], {z, 50, 220}];
f3 = ListPlot[K1, PlotStyle -> {Red, Thick}];
Show[f3, Y3, AxesOrigin -> {0, -0.1}, PlotRange -> All, Frame -> {True, True, True, True},
  FrameLabel -> {Text@Style["Heliocentric distance (in solar radii)", Bold, {Blue}],
    Text@Style[" B(nT)", Bold, {Blue}]}, LabelStyle -> {FontSize -> 25, Bold, {Black}}]
(* Plotting end profile of B along with the interpolating polynomial *)
c = Y[215]; (* Extrapolated value at 1 AU *)

(* 2. Extrapolation of B value at 1 AU by fitting *)
V = FindFit[K1, {w/(1^(m*x)) + n}, {w, l, m, n}, x];
(* Fitting the end profile with function w1-mx+n *)
U = Function[x, w/(1^(m*x)) + n] /. V
u3 = Plot[U[x], {x, 30, 215}, PlotRange -> All];
Show[f3, u3, AxesOrigin -> {0, -0.1}, PlotRange -> All, Frame -> {True, True, True, True},
  FrameLabel -> {Text@Style["Heliocentric distance (in solar radii)", Bold, {Blue}],
    Text@Style[" nT", Bold, {Blue}]}, LabelStyle -> {FontSize -> 15, Bold, {Black}}]
(* plotting data points of B along with the fit *)
t = U[215]; (* Extrapolated value at 1 AU *)
```

Bibliography

- [1] Arya Akmal, John C Raymond, Angelos Vourlidas, Barbara Thompson, A Ciaravella, Y-K Ko, M Uzzo, and R Wu. Soho observations of a coronal mass ejection. *The Astrophysical Journal*, 553(2):922, 2001.
- [2] Paul M Bellan. *Fundamentals of Plasma Physics*. Cambridge University Press, 2008.
- [3] Daniel Benjamín Berdichevsky. On fields and mass constraints for the uniform propagation of magnetic-flux ropes undergoing isotropic expansion. *Solar Physics*, 284(1):245–259, nov 2012.
- [4] DH Boteler, RJ Pirjola, and H Nevanlinna. The effects of geomagnetic disturbances on electrical systems at the earth’s surface. *Advances in Space Research*, 22(1):17–27, 1998.
- [5] L. F. Burlaga. Magnetic clouds and force-free fields with constant alpha. *Journal of Geophysical Research: Space Physics*, 93(A7):7217–7224.
- [6] James Chen. Theory of prominence eruption and propagation: Interplanetary consequences. *Journal of Geophysical Research: Space Physics*, 101(A12):27499–27519.
- [7] James Chen. Effects of toroidal forces in current loops embedded in a background plasma. *The Astrophysical Journal*, 338:453–470, 1989.
- [8] A Ciaravella, JC Raymond, F Reale, L Strachan, and G Peres. 1997 december 12 helical coronal mass ejection. ii. density, energy estimates, and hydrodynamics. *The Astrophysical Journal*, 557(1):351, 2001.
- [9] TG Forbes. A review on the genesis of coronal mass ejections. *Journal of Geophysical Research: Space Physics*, 105(A10):23153–23165, 2000.

- [10] David A Garren and James Chen. Lorentz self-forces on curved current loops. *Physics of plasmas*, 1(10):3425–3436, 1994.
- [11] Timothy Howard. *Coronal Mass Ejections*. Springer, 2011.
- [12] B Kliem and T Török. Torus instability. *Physical Review Letters*, 96(25):255002, 2006.
- [13] Ashok Kumar and D. M. Rust. Interplanetary magnetic clouds, helicity conservation, and current-core flux-ropes. *Journal of Geophysical Research: Space Physics*, 101(A7):15667–15684.
- [14] Yolande Leblanc, George A Dulk, and Jean-Louis Bougeret. Tracing the electron density from the corona to 1 au. *Solar Physics*, 183(1):165–180, 1998.
- [15] J-Y Lee, JC Raymond, Y-K Ko, and K-S Kim. Three-dimensional structure and energy balance of a coronal mass ejection. *The Astrophysical Journal*, 692(2):1271, 2009.
- [16] Y Liu, JD Richardson, JW Belcher, JC Kasper, and HA Elliott. Thermodynamic structure of collision-dominated expanding plasma: Heating of interplanetary coronal mass ejections. *Journal of Geophysical Research: Space Physics*, 111(A1), 2006.
- [17] Stig Lundquist. Magnetohydrostatic fields. *Ark. Fys.*, 2:361–365, 1950.
- [18] K. Miyamoto. *Plasma physics for nuclear fusion*. 1980.
- [19] NA Murphy, JC Raymond, and KE Korreck. Plasma heating during a coronal mass ejection observed by the solar and heliospheric observatory. *The Astrophysical Journal*, 735(1):17, 2011.
- [20] C. E. Myers, M. Yamada, H. Ji, J. Yoo, J. Jara-Almonte, and W. Fox. Laboratory study of low- forces in arched, line-tied magnetic flux ropes. *Physics of Plasmas*, 23(11):112102, 2016.
- [21] Jiong Qiu, Haimin Wang, CZ Cheng, and Dale E Gary. Magnetic reconnection and mass acceleration in flare-coronal mass ejection events. *The Astrophysical Journal*, 604(2):900, 2004.
- [22] K Sasikumar Raja, Prasad Subramanian, R Ramesh, Angelos Vourlidas, and Madhusudan Ingale. Turbulent density fluctuations and proton heating rate in the solar wind from 9–20 rL. *The Astrophysical Journal*, 850(2):129, 2017.

- [23] Nishtha Sachdeva, Prasad Subramanian, Angelos Vourlidas, and Volker Bothmer. Cme dynamics using stereo and lasco observations: The relative importance of lorentz forces and solar wind drag. *Solar Physics*, 292(9):118, 2017.
- [24] HC Spruit. Essential magnetohydrodynamics for astrophysics. *arXiv preprint arXiv:1301.5572*, 2013.
- [25] Prasad Subramanian, KP Arunbabu, Angelos Vourlidas, and Adwiteey Mauriya. Self-similar expansion of solar coronal mass ejections: Implications for lorentz self-force driving. *The Astrophysical Journal*, 790(2):125, 2014.
- [26] Prasad Subramanian and Angelos Vourlidas. Driving currents for flux rope coronal mass ejections. *The Astrophysical Journal*, 693(2):1219, 2009.
- [27] MS Venzmer and V Bothmer. Solar-wind predictions for the parker solar probe orbit-near-sun extrapolations derived from an empirical solar-wind model based on helios and omni observations. *Astronomy & Astrophysics*, 611:A36, 2018.
- [28] Yuming Wang, Jie Zhang, and Chenglong Shen. An analytical model probing the internal state of coronal mass ejections based on observations of their expansions and propagations. *Journal of Geophysical Research: Space Physics*, 114(A10), 2009.